2008

Impact of Electron-Electron Spin Interaction on Electron Spin Relaxation of Nitroxide Diradicals and Tetraradical in Glassy Solvents Between 10 and 300 K

Hideo Sato
University of Denver

Velavan Kathirvelu
University of Denver

Gaëlle Spagnol
University of Nebraska-Lincoln

Suchada Rajca
University of Nebraska-Lincoln, srajca1@unl.edu

Andrzej Rajca
University of Nebraska - Lincoln, arajca1@unl.edu

See next page for additional authors

Sato, Hideo; Kathirvelu, Velavan; Spagnol, Gaëlle; Rajca, Suchada; Rajca, Andrzej; Eaton, Sandra S.; and Eaton, Gareth R., "Impact of Electron-Electron Spin Interaction on Electron Spin Relaxation of Nitroxide Diradicals and Tetraradical in Glassy Solvents Between 10 and 300 K" (2008). *Andrzej Rajca Publications*. 11.
http://digitalcommons.unl.edu/chemistryrajca/11

Authors
Hideo Sato, Velavan Kathirvelu, Gaëlle Spagnol, Suchada Rajca, Andrzej Rajca, Sandra S. Eaton, and Gareth R. Eaton

Published in final edited form as:
J Phys Chem B. 2008 March 13; 112(10): 2818–2828. doi:10.1021/jp073600u.

Impact of Electron-Electron Spin Interaction on Electron Spin Relaxation of Nitroxide Diradicals and Tetraradical in Glassy Solvents Between 10 and 300 K

Hideo Sato[†], **Velavan Kathirvelu**[†], **Gaëlle Spagnol**[‡], **Suchada Rajca**[‡], **Andrzej Rajca**[‡], **Sandra S. Eaton**[*,†], and **Gareth R. Eaton**[†]

[†]Department of Chemistry and Biochemistry, 2101 East Wesley Avenue, University of Denver, Denver, Colorado 80208-2436

[‡]Department of Chemistry, University of Nebraska, Lincoln, Nebraska 68588-0304

Abstract

To determine the impact of electron-electron spin-spin interactions on electron spin relaxation rates, $1/T_1$ and $1/T_m$ were measured for nitroxide monoradical, diradical, and tetraradical derivatives of 1,3-alternate calix[4]arenes, for two pegylated high-spin nitroxide diradicals, and for an azine-linked nitroxide diradical. The synthesis and characterization by SQUID (superconducting quantum interference device) magnetometry of one of the high-spin diradicals, in which nitroxides are conformationally constrained to be coplanar with the *m*-phenylene unit, is reported. The interspin distances ranged from about 5-9 Å, and the magnitude of the exchange interaction ranged from >150 to >0.1 K. $1/T_1$ and $1/T_m$ were measured by long-pulse saturation recovery, three-pulse inversion recovery, and two-pulse echo decay at X-band (9.5 GHz) and Q-band (35 GHz). For a diradical with interspin distance about 9 Å, relaxation rates were only slightly faster than for a monoradical with analogous structure. For interspin distances of about 5-6 Å, relaxation rates in glassy solvents up to 300 K increased in the order monoradical < diradical < tetraradical. Modulation of electron-electron interaction enhanced relaxation via the direct, Raman, and local mode processes. The largest differences in $1/T_1$ were observed below 10 K, where the direct process dominates. For the three diradicals with comparable magnitude of dipolar interaction, $1/T_m$ and $1/T_1$ were faster for the molecules with more flexible structures. Relaxation rates were faster in the less rigid low-polarity sucrose octaacetate glass than in the more rigid 4:1 toluene/chloroform or in hydrogen-bonded glycerol glasses, which highlights the impact of motion on relaxation.

1. Introduction

Nitroxide radicals have been widely used as probes of molecular dynamics, including motion of spin labels on polymers and biomolecules, probes in membranes, and details of molecule tumbling in liquids. The anisotropy of the nitroxide *g* values and hyperfine couplings make EPR spectra of nitroxide radicals at various microwave frequencies sensitive reporters of molecular motion. The impact of motion on electron spin relaxation rates $1/T_2$ and phase memory dephasing rate $1/T_m$ has been thoroughly analyzed, especially by the Freed lab.[1,2] Motion partially averages anisotropy in glasses or solids, resulting in changes in $1/T_m$.[3,4] Electron spin relaxation rates are important for many applications of free radicals. For example, site-directed mutagenesis, spin labeling, and EPR double-resonance methods combine to use

---

[*]Corresponding author. Phone: 303-871-3102. Fax: 303-871-2254. E-mail: seaton@du.edu.

the interaction between two nitroxide spin labels to measure distances between sites in proteins.[5-7] Both $1/T_1$ and $1/T_m$ affect the selection of experimental parameters for the distance measurements. Nitroxide polyradicals with $S > ½$ are under investigation as NMR relaxation enhancement reagents,[8] and there is interest in dinitroxides as dynamic nuclear polarization agents.[9] Optimization of each of these applications depends upon an understanding of the electron spin relaxation properties. Because of the many possible electron spin relaxation mechanisms, and the wide range of motional regimes in which nitroxides radicals are used, fundamental studies of spin relaxation are needed in many solvents, over large temperature ranges, and at multiple microwave frequencies to provide confident bases for predicting relaxation mechanisms and rates for a new radical or a previously studied radical in a new environment. Very little is known about relaxation rates and mechanisms involved in interactions of two or more radicals.

For nitroxide monoradicals in a glassy or crystalline matrix the dominant contributions to relaxation are the Raman process and a local mode, which modulate spin-orbit coupling.[10] As the matrix softens, molecular reorientation rates increase and processes that modulate anisotropic hyperfine interaction make significant contributions to relaxation.[11,12] It is well-documented that the interaction of a nitroxide radical with a more rapidly relaxing center results in relaxation enhancement that can be used to determine interspin distances,[13,14] but much less is known about the relaxation enhancement that arises from nitroxide-nitroxide interaction. To address this question a series of diradicals and a tetraradical (Figure 1, Table 1) were studied.

Tetraradical **1a**, diradical **1b**, and related monoradical **1c** have the 1,3-alternate calix[4]arene structure. In tetraradical **1a**, the exchange coupling between nitroxides attached to adjacent phenyl rings is antiferromagnetic ($J_1/k \sim -1$ K).[15] The through-space coupling between the diagonal nitroxides at the N···N distance of 5-6 Å in **1a** and **1b** is antiferromagnetic, with a matrix-dependent coupling strength of $J_2/k \sim -1$ K.[15] In tetraradical **1a**, the exchange interactions lead to three $S = 1$ manifolds and one $S = 2$ manifold that are thermally populated throughout the temperature range studied; two of the $S = 1$ manifolds are degenerate.[15]

The two *m*-phenylene-based high-spin diradicals **2a** and **2b** were investigated to determine the impact of structure and stronger exchange interaction. Diradical **2a** was designed and synthesized to possess a relatively rigid structure with planar conformation and very strong ferromagnetic coupling, to ensure complete population of the $S = 1$ state, even at room temperature.[16] Diradicals **2b** and **2a** have ferromagnetic exchange couplings $J_1/k \approx 150$ K and >150 K, respectively. The azine-linked diradical **3** has a longer interspin distance (about 8-9 Å)[17-19] and weaker exchange interaction than for diradicals **1b**, **2a**, or **2b**. For diradicals **1b**, **2a**, **2b**, and **3** *J* is larger than the EPR quantum and anisotropies, transitions are observed only within the $S = 1$ manifold, and the energies of the EPR transitions are not strongly dependent on *J*.

2. Methods

2.1. Sample Preparation

4-Hydroxy-2,2,6,6-tetramethylpiperidine-1-oxyl (tempol), α,*γ*-bisdiphenylene-*β*-phenylallyl (BDPA), and Fremy's salt ($(SO_3)_2NO^{2-}(K^+)_2$) were used as received from Aldrich Chemical Co. Tetraradical **1a** and diradical **1b** were prepared as previously reported;[15] similar methods were used for preparation of the corresponding calix[4]arene monoradical **1c** (Supporting Information). Diradical **2b** was prepared using methods similar to those for the previously reported monopegylated diradical;[20] synthetic details and magnetic characterization for **2b** will be reported elsewhere. Diradical **3** was prepared as reported previously.[21]

Diradical **2a** was prepared from the corresponding diamine (1:1 mixture of diastereomers).[22] *m*-Chloroperbenzoic acid (57.6 mg, 0.326 mmol, 11.7 mL of 27.8 mM in dichloromethane, 4.1 equiv) was added to the diamine[22] (50.0 mg, 0.0796 mmol, 1 equiv) in dichloromethane (5.0 mL) at 0 °C, in two portions (2 + 2.1 equiv), at an interval of 1 h. After an additional 1 h at 0 °C, the orange reaction mixture was transferred with acetone, concentrated in vacuo, and then filtered through deactivated silica gel (pentane/acetone, 7:3) at low temperature (-20 °C). (Silica gel was deactivated using 5% triethylamine in pentane as described previously.[16]) The orange band of the product was collected, to give nitroxide diradical **2a** as a red oil (28.0 mg, 53%). Because the starting diamine was a mixture of diastereomers, and only this particular band exhibits EPR spectra corresponding to a diradical, it is assumed that **2a** is isolated as a mixture of diastereomers with indistinguishable EPR spectra.

For magnetic studies of pegylated diradical **2a** in solution, a 2:1 ethanol/water solvent mixture was selected, as it provides good solubility and matrix rigidity for magnetic studies and it permits obtaining well-resolved EPR spectra. Diradical **2a** (0.41 or 0.80 mg) was placed in a homemade 5 mm o.d. EPR-quality quartz tube (superconducting quantum interference device (SQUID) tube), modified to possess a thin bottom, which is 6 cm from the end of the tube.[15] Following vacuum transfers of solvent (~0.1 mL), the tube was flame-sealed under vacuum. For neat samples, diradical **2a** (7.89 mg) was loaded into the SQUID tube using acetone, to form a small band of viscous oil at the thin bottom. The open tube was directly attached to the sample holder. Following the measurements, the tube was completely emptied and ^{1}H NMR spectra in benzene-d_6 were obtained, indicating 10 mol % of residual acetone. Identical sequences of measurements were carried out on the empty tube to provide point-by-point correction for diamagnetism; additional correction for diamagnetism was based upon Pascal constants (χdia = -4.16×10^{-4} emu mol^{-1}).

For EPR studies, a 4:1 toluene/$CHCl_3$ solvent mixture was selected because it forms a glass with a softening temperature of about 130 K and each of the radicals is soluble in this mixture. To minimize the impact of intermolecular radical-radical interactions, concentrations were less than 1 mM: tetraradical **1a**, 0.21 mM; diradical **1b**, 0.96 or 0.18 mM; monoradical **1c**, ~0.5 mM; diradical **2a**, 0.56 mM; diradical **2b**, 0.55 mM; diradical **3**, 0.5 mM. Each of the radicals also dissolves in sucrose octaacetate, which forms a glass with glass transition temperature at 298 K.[23] Weighed portions of radical and sucrose octaacetate powder were mixed by gentle grinding. The mixtures were placed in 1 mm i.d. capillaries, evacuated, and flame-sealed. The mixtures were melted briefly with a heat gun and cooled quickly in water to form a glass. The brief melting period may not be long enough to give a uniform distribution of radicals in the glass, but prolonged heating causes loss of EPR signal. A single capillary tube was used for Q-band experiments. A bundle of three or four capillaries was used for X-band measurements. The concentrations of the BDPA samples in sucrose octaacetate glasses were determined by comparison of the integrated intensities at 125 K with that for a known concentration of tempol in 1:1 water/glycerol at the same temperature. A solution of Fremy’s salt in 1.0 M KOH solution was mixed 1:1 with glycerol, transferred to a 4 mm o.d. EPR tube, and stored in liquid nitrogen.

2.2. SQUID Magnetometry

A 5 T ac/dc SQUID magnetometer (Quantum Design MPMS5S), with continuous temperature control and operating in the dc-mode, was used. Magnetization (M) was measured as a function of magnetic field (H = 0-5 × 10^4 Oe and T = 1.8, 3, and 5 K) and temperature (T = 1.8-290 K at H = 30 000, 5000, or 500 Oe).

2.3. EPR Spectroscopy

CW spectra, long-pulse saturation recovery (SR) and inversion recovery, and two-pulse spin-echo at X-band and Q-band were recorded on a Bruker E580 with a SuperQFT bridge, split ring resonators, and a Bruker CF935 cryostat. The magnetic field was calibrated using a g value for lithium phthalocyanine of 2.00225.[24] X-band SR measurements also were performed with a locally constructed spectrometer[25] using a TE_{102} rectangular resonator. A Varian flow-through dewar and temperature controller and nitrogen gas cooled with liquid nitrogen were used to obtain temperatures above 100 K. Temperatures between 10 and 90 K were obtained with liquid helium, an Oxford ESR900 flow cryostat, and an ITC601 temperature controller. For the SR experiments the lengths of the saturating pulses were long relative to T_1 to minimize the effects of spectral diffusion. Above about 80 K the time constants obtained by inversion recovery and SR are the same, but at lower temperatures shorter time constants were obtained by inversion recovery, which is attributed to contributions from spectral diffusion. The Q of the rectangular resonator is about 3000, and the dead time following a pulse for SR is about 1.5 μs. The pulse sequence for inversion recovery was 180-T_{var}-90-τ-180-τ-echo, and for two-pulse echo it was 90-τ-180-τ-echo. Most experiments were performed with an 80 ns π pulse. For monoradical samples at temperatures where instantaneous diffusion made significant contributions to echo decays, smaller turning angles were used. The temperature dependence of relaxation for monoradicals was monitored in the center of the spectrum where contributions from g_{xx} and g_{yy} dominate, and for diradicals it was monitored at the low-field position for $D_{\perp}$.

At Nebraska, routine CW spectra were obtained using a Bruker EMX instrument, equipped with a frequency counter and nitrogen flow temperature control (130-300 K).

CW line shapes in glassy solution were simulated using XSophe.[26] The g values and nitrogen hyperfine splittings are typical of nitroxide radicals (Supporting Information Table S1). It was assumed that the dipole-dipole interspin vector was along a principal axis of the nitroxide g and A tensor, which was adequate to determine the magnitude of the dipolar couplings. Further refinements involving changes in the relative orientations of the axes were not attempted. The dipolar splittings and line widths are summarized in Table 2. The point dipole interspin distances for **1b**, **2a**, and **2b** (Table 1) were calculated from the dipolar splittings.

2.3.1. Determination of Value of S by Pulse Turning Angle—The microwave power required to achieve a 90° turning angle depends on the value of S.[27] The turning angle can be calculated from the expressions $\theta = c\gamma B_1 t_p$ where γ is the magnetogyric ratio, B_1 is the microwave magnetic field, t_p is the length of the pulse, and $c = [S(S + 1) - m_s(m_s + 1)]^{1/2}$. The B_1 required to produce a 90° pulse decreased in the order monoradicals (S = ½) > diradicals (S = 1) > tetraradical (mixture of S = 1 and S = 2), which is consistent with the assignments of the spin states. The precision of the turning angle experiments was not sufficient to characterize the populations of S = 1 and S = 2 for the tetraradical.

2.4. Analysis of Saturation Recovery and Inversion Recovery Curves

Preliminary data analysis was performed by fitting with a single exponential. However, the recovery curves for nitroxide radicals in glassy matrixes are not single exponentials due to the orientation dependence of vibrations, molecular motion, and spin-orbit coupling.[28] The recovery curves were modeled with a log-normal distribution of T_1 as defined by eq 1[29]

$$\text{log}-\text{normal distribution}=\sum_{i=1}^{n}\frac{1}{\sigma\sqrt{2\pi}}\exp\left[-\frac{\left(\log\left[T_1^i\right]-\log\left[b\right]\right)^2}{2\sigma^2}\right]\exp\left[-t/T_1^i\right] \tag{1}$$

where σ is the standard deviation of the distribution on the logarithmic scale and b is the center of the distribution.

Analogous to the uniform penalty model (UPEN),[30,31] the relaxation time distribution is sampled at evenly spaced points on a logarithmic scale between minimum and maximum T_1 values that are determined by the longest and shortest times at which data were acquired, the centers of the distributions, and the distribution widths. The Levenberg-Marquardt method, as implemented in Mathematica, was used to find the solutions. Increasing the number of points in the distribution from 50 to 200 gave no detectable improvement in the fit to the recovery curves, so the number of points was set at 50.

For magnetically dilute nitroxides in glassy solvents the distribution width σ has been found to be 0.27 ± 0.3 and approximately independent of temperature below the glass transition temperature. The SR curves for diradicals (**1b**, **2a**, **2b**, **3**) at magnetic field positions where the monoradical impurity is not detected in the CW spectra and SR curves for monoradical **1c** fit well with a single log-normal distribution with $\sigma = 0.27 \pm 0.4$. The σ for tetraradical **1a** was significantly larger (0.46) than those of the diradical and monoradicals. Therefore, the inversion recovery and SR curves for diradicals and monoradicals were analyzed with $\sigma = 0.27$, whereas data for the tetraradical were analyzed with $\sigma = 0.46$. The value for T_1 calculated at the center of the distribution is about 0.8 ($\sigma = 0.27$) or 0.54 ($\sigma = 0.46$) times the approximate value found by fitting a single exponential to the recovery curves. The quality of the fits to the data with distributions of exponentials is shown in Supporting Information Figure S1. The wider distributions of relaxation rates for the tetraradical than for the monoradical or diradicals (Figure S1) may be due to modulation of electron-electron dipolar interactions for a larger number of conformations or to different values of T_1 for the three triplet manifolds and one quintet manifold in the tetraradical.[15]

In the center of the spectra for diradicals **1b**, **2a**, or **3** there are overlapping contributions from monoradical and diradical, so the SR curves were modeled as the sum of two log-normal distributions as described by eqs 1 and 2

$$\text{weighteddistribution} = C1\,(\text{distribution}\,1) + C2\,(\text{distribution}\,2) \tag{2}$$

where $C1$ and $C2$ are the coefficients for the two distributions. For the SR experiments the relative intensities of the monoradical and diradical signals were estimated by integration of the CW spectra, and the coefficients for analysis of the inversion recovery curves were calculated from field-swept echo-detected spectra. In the analyses of the composite signals the relaxation times for the diradical were fixed at the values observed at the lower-field g_{xx} turning point, where only diradical contributed. Fitting to the sums of distributions of exponentials gave a clearer separation of the contributions from monoradical and diradical than could be obtained with the sum of two exponentials. The trends in temperature dependence of $1/T_1$ are independent of the model that was used to fit the recovery curves.

2.5. Analysis of Two-Pulse Spin Echo Decays

Single exponentials were fitted to the two-pulse echo decays. Oscillations due to echo envelope modulation cause some uncertainty in the time constants. In the center of the spectra for diradical **1b**, **2a**, or **3** there are overlapping contributions from monoradical and diradical, so the echo decay curves were modeled as the sum of two exponentials. The ratios of the components were estimated from the echo-detected field-swept spectra.

Echo decays also were fitted with stretched exponentials

$$Y(\tau) = Y_0 \exp\left(-\left(\frac{2\tau}{T_\mathrm{m}}\right)^x\right) \tag{3}$$

where Y_0 is the amplitude at time zero and τ is the time between pulses.

The echo decay time constant is designated as T_m to indicate that it includes processes such as molecular motion and instantaneous diffusion that take spins off resonance, as well as electron-electron spin-spin interaction. Deviations of the value of x (eq 3) from 1 can arise from distributions of exponentials or from changes in the mechanisms of echo dephasing.[32] Discussions of trends in $1/T_m$ are based primarily on single-exponential fits because the introduction of two parameters, T_m and x, leads to greater scatter.

2.6. Model for Temperature Dependence of $1/T_1$

The temperature-dependent relaxation rates were modeled as the sum of contributions from the direct, Raman, and local modes (eq 4)[12,33]

$$\frac{1}{T_1}=A_{\mathrm{direct}}\,(T+b)+A_{\mathrm{Ram}}\left(\frac{T}{\theta_{\mathrm{D}}}\right)^9 J_8\,(\theta_{\mathrm{D}}/T)+A_{\mathrm{loc}}\frac{\exp\,[\Delta_{\mathrm{loc}}/T]}{(\exp\,[\Delta_{\mathrm{loc}}/T]-1)^2} \tag{4}$$

where T is temperature in Kelvin, A_{direct} and b are the coefficients for the contribution from the direct process, A_{Ram} is the coefficient for the contribution from the Raman process, θ_D is the Debye temperature, J_8 is the transport integral, $J_8\,(\theta_{\mathrm{D}}/T)=\int_0^{\theta_{\mathrm{D}}/T} x^8\left(\mathrm{e}^x/(\mathrm{e}^x-1)^2\right)\mathrm{d}x$, A_{loc} is the coefficient for the contribution from local mode, and Δ_{loc} is the energy of the local mode. For the diradicals and tetraradicals the coefficients include contributions from modulation of both spin-orbit coupling and electron-electron interaction. Each of these processes results in a distinctive temperature dependence of $1/T_1$. Above the glass transition temperature, molecular reorientation provides effective relaxation enhancement, which is not included in the modeling. The parameters obtained by fitting eq 4 to the experimental data are summarized in Table 3. When the Debye temperatures was allowed to vary, the values in 4:1 toluene/$CHCl_3$ were 104 ± 15, so θ_D was fixed at 100 K to facilitate comparison of A_{Ram}. The assignment of the process that contributes in sucrose octaacetate glasses above about 100 K as a local mode, rather than a thermally activated process, is based on the similarity of the relaxation rates at X-band and Q-band.[12] The energy of the local mode was estimated as 950 K (650 cm^{-1}) for diradical **2a** in sucrose octaacetate, for which data were measured up to 300 K. The same value of Δ_{loc} = 950 K was used for **2a** in glycerol to permit comparison of the coefficients, A_{loc}.

2.7. DFT Calculations

The optimized geometries and vibrational frequencies of nitroxide diradicals were calculated at the unrestricted DFT level (6-31G(d), UB3LYP functional) with a Windows version of Gaussian 03.[34] Calculations were performed for **4a** and **4b**, as models of **2a** and **2b** with fewer atoms. The potential energy surfaces near the minimum energy of the triplet states are nearly flat. Even with the maximum root-mean-square (rms) forces an order of magnitude or more below the “tight” thresholds of Gaussian 03, small displacements with negligible energy changes are still estimated for each structure.

For **4a**, frequencies were calculated after completed geometry optimization with the standard thresholds of Gaussian 03. After 138 additional geometry optimization steps, forces and displacements remained essentially unchanged and the forces were at least 1 order of magnitude below the “tight” thresholds. This geometry was in good agreement with the X-ray structure of **4a**.[16] For anti-**4b** and syn-**4b**, the geometry optimizations were completed on the basis of negligible forces with respect to “tight” thresholds, and these geometries were used for frequency calculations. For π-conjugated organic molecules, the frequencies calculated at the

B3LYP/6-31(d) level and then scaled by 0.97 show good agreement with experimental data.[34]

3. Results and Discussions

3.1. Magnetic Studies

The magnetization (M) versus magnetic field (H) data at low temperatures (T = 1.8, 3, 5 K) for diradical **2a** in EtOH/water and in the solid state could be fit with the Brillouin functions with a mean-field parameter ($\theta < 0$), i.e., M versus $H/(T - \theta)$ (Figures 2 and 3, inset plots). The fits have two variable parameters, i.e., total spin (S) and magnetization at saturation (M_{sat}); the mean-field parameter θ is adjusted until the M/M_{sat} versus $H/(T - \theta)$ plots overlap at all temperatures. The quality of the fits is much better for the dilute solution samples, which possess negligibly small values of $|\theta| < 0.1$ K, indicating nearly ideal paramagnetic behavior. Since $|\theta|$ in dilute solution is smaller by a factor of 10 than the solid-state values, it is almost certain that the values of $\theta < 0$ correspond to intermolecular antiferromagnetic coupling. For both solution and solid-state samples, the values of $S \approx 1.0$, determined from the curvature of the Brillouin plots, indicate a triplet ($S = 1$) ground state for **2a**.

The χT versus T plots support the magnetization results and provide additional information about the strength of ferromagnetic coupling (singlet-triplet energy gap, $2J/k$) for **2a** (Figures 2 and 3, main plots). In particular, the downward curvature of the χT versus T plot is much smaller in solution, compared to the solid state. For solid **2a**, the χT versus T plot in the high-temperature range is flat with $\chi T \approx 0.96$ emu K mol^{-1}, which is near the expected value of 1.00 emu K mol^{-1} for a diradical that is entirely in an $S = 1$ state. This result implies that even at room temperature **2a** is entirely in an $S = 1$ state, i.e., $2J/k \gg 300$ K. For **2a** in EtOH/H$_2$O, the χT versus T plot is flat up to 150 K. The highest temperature of measurement is limited by the rigidity of the solvent matrix; therefore, only a lower limit, $2J/k \gg 200$ K, for the strength of ferromagnetic coupling can be estimated.

3.2. Comparison of CW EPR Spectra

The X-band EPR spectrum of monoradical **1c** in 4:1 toluene/CHCl$_3$ at 60 K (Figure 4a) is typical of nitroxides in frozen or glassy solution. The nitrogen hyperfine coupling (A_{zz} = 3.08 mT at 60 K) is the dominant interaction that defines the spectral shape. The $|\Delta m_s| = 1$ spectrum of diradical **1b** at 50 K (Figure 4a) is dominated by the zero-field splitting[15] with $|D_{\|}|$ and $|D_{\perp}|$ of 30.2 and 15.1 mT, respectively, which corresponds to a point-dipole distance of 5.7 Å. For nitroxides the axis designations are x (along the NO bond), y (perpendicular to NO bond and to π-orbital), and z (along the nitrogen π-orbital).[35] The interspin vector is along the z-axis of the nitroxide, which is consistent with the known structure of the diradical (Figure 1). The line widths for diradical **1b** are too large to permit resolution of nitrogen hyperfine interaction. For **1b**, a well-resolved $|\Delta m_s| = 2$ (half-field) transition is observed with a nitrogen hyperfine splitting that is half of the value for the monoradical. The observation of a half-field transition is characteristic of dipolar coupled spins.[19] The monoradical line shape in the center of the spectrum of the diradical **1b** is due to a small impurity of monoradical.

The room-temperature fluid solution spectrum of tetraradical **1a** is a well-resolved nine-line spectrum that is characteristic of strong exchange interaction that makes coupling to all four nitrogens equivalent.[15] In glassy 4:1 toluene/CHCl$_3$ at 50 K the spectrum of tetraradical **1a** is an incompletely resolved single line with a peak-to-peak line width of about 2.0 mT (Figure 4a), which is much narrower than the spectrum of diradical **1b** and shows no resolved dipolar coupling.[15] The tetraradical can be viewed as two pairs of radicals. Within each pair the interspin distance is about 5-6 Å, and the radicals in different pairs are separated by about 9-10 Å.[15] When the magnetic field is along the interspin vector for one pair of radicals, it is approximately perpendicular to the interspin vector for the other pair, so the two intrapair dipolar couplings are inequivalent. The absence of resolved dipolar splitting in the spectrum for **1a** (Figure 4a) indicates that the exchange interaction between the four paramagnetic centers is strong enough to average the inequivalent dipolar couplings, which is consistent with the value of about $|J/k| \sim 1$ K determined by magnetic susceptibility.[15]

The room-temperature fluid solution spectrum of diradical **3** exhibits five-line hyperfine splitting that is characteristic of strong exchange and equivalent coupling to both nitroxide nitrogens. The magnitude of the dipolar coupling for **3** is smaller than for diradicals **1b**, **2a**, or **2b**, so the rigid-lattice spectrum extends over a smaller range of magnetic fields (Figure 4b). A single-crystal EPR study of **3** reported $D_{zz} = 3.4$ (0.1), $D_{yy} = 1.53$ (0.04), and $D_{xx} = 1.87$ (0.05) mT.[17] These dipolar couplings are of the same order of magnitude as the nitrogen hyperfine splittings, which causes extensive overlap of transitions. In addition there may be several conformations of the nitroxide rings, which make simulation of the CW spectra difficult.

Figure 4b also shows the CW spectra of diradicals **1b**, **2a**, and **2b** in sucrose octaacetate glass at 294 K. The room-temperature spectrum of **1b** is broader than at 50 K, which is attributed to increased motion and distributions of geometries in the relatively flexible diradical. For diradical **2a** the maximum dipolar splitting is along the g_{yy} axis (Figure 4b and Supporting Information Figure S2) which is consistent with the structure shown in Figure 1. Nitrogen hyperfine splitting of five lines separated by $A_{zz}/2$ is observed along g_{zz}, consistent with $J \gg A_{zz}$. For diradical **2b** the maximum dipolar coupling also is along g_{yy} (consistent with the structure shown in Figure 1), and the nitrogen hyperfine interaction is partially resolved along g_{zz}. The weak outermost lines in the spectrum of **2b** that are not reproduced by the simulation (Figure 4b) are attributed to a minor conformer with larger D_{yy}. A second conformer also was observed for an analogous diradical in polar solvents.[20] The smaller line widths for **2a** than for the other diradicals at both 70 K in toluene/$CHCl_3$ and at 294 K in sucrose octaacetate and the small change in line widths between 86 and 294 K in sucrose octaacetate (Table 1) are consistent with greater rigidity of this diradical.

Even for the relatively rigid diradical **2a** the CW spectrum changes with temperature (Supporting Information Figure S3a) because of the temperature dependence of the D_{xx} and D_{zz} components of the dipolar coupling (Supporting Information Figure S3b). The temperature-dependent impact of libration on A_{zz} for nitroxide monoradicals has been described,[36-38] and it is proposed that comparable effects occur for the dipolar couplings. Motion around the y-axis averages the x and z components leaving the y component unchanged. This averaging corresponds to libration of the plane of the core of the molecule, which is plausible even in a glassy host.

3.3. Spin Echo Dephasing, $1/T_m$

The spin echo dephasing rate, $1/T_m$, includes contributions from all processes that take spins off resonance on the time scale of the experiment and therefore provides insight into molecular motion. Low-amplitude vibrations (librations) modulate the orientation of the magnetic axes relative to the external magnetic field and enhance spin echo dephasing proportional to anisotropy. This effect is greatest at positions in the spectrum where a change in orientation causes the greatest change in resonant field.[37,39] For monoradicals in temperature ranges where librations contribute to dephasing, rates are slowest near the principal magnetic axes and faster at intermediate positions.[12,39,40] In diradicals, motions that modulate the interspin distance and/or orientation of the interspin vector change the resonance field, which can also contribute to echo dephasing.

3.3.1. Temperature Dependence of 1/T_m—The temperature dependence of 1/T_m for **1c** (Figure 5) is typical of nitroxide monoradicals.[12] Relaxation rates for **3_mono** (data not shown) are similar to those for **1c**. At temperatures less than ~50 K, mutual spin-flips of neighboring protons (nuclear spin diffusion) dominate the relaxation and there is little temperature dependence.[3,32] When the low-temperature data were fitted with eq 3, T_m was 2-6 μs and the exponent x approached 2 as temperature was decreased. The increase in 1/T_m for **1c** and **3_mono** above about 70 K is due to rotation of methyl groups at rates comparable to inequivalences in the electron-proton couplings that are averaged by rotation.[40,41] For radicals without methyl groups such as Fremy's salt, 1/T_m shows little temperature dependence below about 110 K (Figure 5), which supports the assignment of the relaxation enhancement for **1c** to methyl rotation.

Below about 20 K the relaxation rates, 1/T_m, for diradicals **1b**, **2a**, **2b**, **3** and tetraradical **1c** are similar to those for monoradicals **1c**, **3_mono**, and Fremy's salt ($(SO_3)_2NO^{2-}$), which indicates that electron-electron dipolar interaction does not dominate the low-temperature limiting values of 1/T_m. The values of the exponent x (eq 3) are about 2 as expected when nuclear spin diffusion dominates dephasing. Above about 20 K the relaxation rates, 1/T_m, increase in the order monoradical **1c** < diradicals **2a** < **2b** < **1b** < tetraradical **1a** (Figure 5). The values of x (eq 3) decrease with increasing temperature (Supporting Information Figure S4) as expected when a dynamic process dominates dephasing. Since the impact of methyl rotation on dephasing for the diradicals or tetraradical is expected to be similar to that for the monoradicals, the enhanced relaxation for the diradicals is attributed to modulation of the electron-electron interactions. The rms values of the dipolar couplings ($\sqrt{0.33\left(D_{xx}{}^2+D_{yy}{}^2+D_{zz}{}^2\right)}$, Table 1) for the three diradicals are **2a**, 20.4 mT; **2b**, 18.3 mT; **1b**, 21.4 mT. Since the dipolar couplings are so similar and the trends in 1/T_m do not correlate with trends in the dipolar couplings or in the values of $|J/h|$, the trend in dephasing rates (**2a** < **2b** < **1b**) is attributed to increasing motion that modulates the dipolar couplings. Although electron-electron dipolar coupling is not observed in the CW spectrum of tetraradical **1a**, modulation of spin-spin interaction is still an effective relaxation process.[42] Modulation of multiple dipolar interactions, exchange interactions, and interconversion between the multiple spin states may contribute to enhanced echo dephasing for **1a**.

3.3.2. Dependence of 1/T_m on Position in the CW Spectrum—The dependence of 1/T_m on position in the spectrum was examined at 86 K, which is a low enough temperature that there is relatively little contribution of methyl rotation to the echo dephasing. Experiments were performed at Q-band to enhance the orientation selection. Even at Q-band the dominant anisotropy is the dipolar splitting. At 86 K the dephasing rates for **2a** increase in the order glycerol < 4:1 toluene/$CHCl_3$ < sucrose octaacetate (Figure 6), which is the order of decreasing glass rigidity. In glycerol 1/T_m for diradical **2a** exhibits little dependence on position in the spectrum, even in the center of the spectrum where **2a_ mono** contributes (Figure 6). The weak dependence on position in the spectrum and the similarity of 1/T_m for monoradical and diradical indicate that motions that modulate the electron-electron dipolar coupling make little contribution to T_m in this relatively rigid glass at 86 K. For the same diradical in the less rigid low-polarity sucrose octaacetate glass the relaxation rates are about 3 times faster than in glycerol and exhibit substantial dependence on position in the spectrum (Figure 6). The rates are slower in the region where the monoradical signal dominates and near the principal axes of the dipolar interaction. Faster rates are observed at intermediate orientations where the same magnitude of motion causes a larger change in resonance field. This is the pattern that is expected when modulation of electron-electron dipolar interaction by librational motion makes a substantial contribution to echo dephasing.

3.4. Spin-Lattice Relaxation, $1/T_1$

3.4.1. Temperature Dependence—

The relaxation rates for **3** in 4:1 toluene/$CHCl_3$ and in sucrose octaacetate between about 20 and 298 K are only slightly faster than for **3_mono** (Figure 7). Below about 20 K in sucrose octaacetate the substantial contribution from the direct process is attributed to a nonuniform distribution of radicals in the glass. Between about 20 and 100 K the rates in both solvents are dominated by the two-phonon Raman process.[12] The faster relaxation rates in the low-polarity relatively soft sucrose octaacetate glass than in the polar and more rigid 4:1 toluene/$CHCl_3$ are typical of nitroxide radicals[10,12,28] and demonstrate the impact of the glassy matrix on the phonon modes that contribute to Raman relaxation. Above about 100 K the 4:1 toluene/$CHCl_3$ glass softens, and tumbling-dependent processes make increasingly important contributions to relaxation. By contrast, the sucrose octaacetate remains glassy up to room temperature. The relaxation rates for **3** in sucrose octaacetate between 100 and 300 K are similar at X- and Q-band, which is consistent with assignment of the Raman and local mode processes. The local mode makes increasingly significant contributions at higher temperatures (Figure 7). The similarity in relaxation rates for **3** and **3_mono** in temperature ranges where three different relaxation processes dominate (Figure 7) shows that the modulation of electron-electron interactions of the magnitude that are present in **3** makes only modest contributions to spin lattice relaxation for a nitroxide radical by each of these processes.

The interspin distances are shorter and the exchange interactions larger for **1b**, **2a**, and **2b** than for **3** (Table 1), and the spin-spin interactions have a greater impact on $1/T_1$ than for **3** (Figure 8). The largest differences in relaxation rates are observed at the lowest temperatures. For comparison with the impact of intermolecular dipolar interaction on $1/T_1$, data are shown in Figure 9 for BDPA in sucrose octaacetate. At low concentration (1.0 or 0.1 mM) the slope of the log-log plot of the relaxation rates versus temperature for BDPA is approximately 2, as expected for the high-temperature limit of the Raman process.[12] At these low BDPA concentrations the direct process makes a small contribution below about 100 K (Figure 9). At higher concentrations the temperature dependence is weaker and can be fit to the eq $1/T_1 = a(T + b)$, which is characteristic of the direct process. For organic radicals in glassy solvents the coefficient a increases linearly with the square of the concentration of the radicals (data not shown). The contribution from the Raman process to the relaxation for dilute BDPA (g = 2.0026) samples (Figure 8) is more than an order of magnitude smaller[10] than the Raman process for the mononitroxide ($g \sim 2.006$) radicals (Figures 7 and 8), so the same magnitude of direct process that is significant for BDPA at 100 K is significant for the nitroxides only at much lower temperatures. Below about 20 K the weak dependence of relaxation rate on temperature for the diradicals and tetraradicals (Figure 8) is attributed to an intramolecular direct process. The bulk concentrations of the diradical and tetraradical samples (<1 mM) were much lower than the 44 mM BDPA sample, so intermolecular contributions from the direct process are much smaller. The coefficients for the direct process increased in the order monoradical < diradicals < tetraradicals (Table 3), which is consistent with increasing local spin concentrations.

Between about 20 and 120 K the dominant contribution to relaxation is the Raman process. For the radicals with the same structures, the coefficients for the Raman process increase in the order monoradical **1c** < diradical **1b** < tetraradical **1a** (Table 3). For these molecules the distribution of phonon energies is approximately constant, and the coefficients for the diradical and tetraradical include modulation of the electron-electron interaction in addition to modulation of the spin-orbit coupling. The order-of-magnitude larger value of A_{Ram} for tetraradical **1a** reflects the larger number of dipolar interactions and/or modulation of the energies of the multiple spin states. For diradical **2a**, A_{Ram} increases in the order glycerol < 4:1 toluene/$CHCl_3$ < sucrose octaacetate which is the order of decreasing intermolecular interactions within the glassy solvents and increasingly softer glasses. For **3_mono**, A_{Ram} is larger than for **1c** or **2a_mono** because of the smaller molecular size.[10] A_{Ram} for **3** is only slightly larger than for **3_mono** (Table 3), consistent with the small impact of electron-electron interaction on $1/T_1$ at this interspin distance.

In 4:1 toluene/$CHCl_3$ above 130 K, the viscosity of the solvent decreases rapidly with increasing temperature and the increasing rates of molecular reorientation provide additional relaxation pathways (Figure 8). This contribution increases in the order monoradical **1c** < diradical **1b** < tetraradical **1a**. In the monoradical, reorientation primarily modulates the anisotropy of the nitrogen hyperfine interaction. For the diradical and tetraradical, reorientation also modulates the electron-electron interactions, which are more numerous for the tetraradical than for the diradical. Above the glass transition temperatures relaxation rates for the diradical and tetraradical are too short to measure by SR.

To characterize processes that contribute to spin lattice relaxation in glasses with higher glass transition temperatures, data were obtained in sucrose octaacetate or glycerol (Figure 10). Between about 20 and 100 K the relaxation rates in these glasses are dominated by the Raman process, and trends in A_{Ram} are similar to trends in 4:1 toluene/$CHCl_3$, **2a** < **2b** < **1b** (Table 3). The larger values of A_{Ram} for **3_mono** and **3** are again attributed to smaller size. The smaller value of A_{Ram} for **2a** in glycerol than in sucrose octaacetate is due to decreased motion in the more rigid glycerol glass.

Above about 100 K the spin lattice relaxation rates for diradical **2a** in glycerol or sucrose octaacetate and for **2b** in sucrose octaacetate are more strongly temperature-dependent than at lower temperatures, which indicates that there is an additional relaxation process. The contributions from this process are the same at X-band and Q-band which is consistent with a local mode and inconsistent with a thermally activated process.[12,43] The values of A_{loc} for **2a** in glycerol and sucrose octaacetate are similar, and much larger than for **2a_mono**. The larger coefficients for the diradicals indicate that this process is dominated by modulation of the electron-electron interaction. The solvent dependence of A_{Ram} and solvent independence of A_{loc} for **2a** is different from the behavior for monoradicals, where the contributions from the Raman and local processes are correlated.[10] The energy of the local mode was estimated as 950 K (650 cm^{-1}). Below about 1450 cm^{-1} there are many vibrational modes for **4a** (a model for **2a**) and for anti-**4b** and syn-**4b** (models for **2b**) that modulate the interspin distance and orientation of the interspin vector. The apparent energy of the local mode falls approximately in the middle of the range and may be a weighted average for several modes. In sucrose octaacetate the larger contribution from the Raman process for **1b** than for **2a** or **2b** (Figure 10) makes the relaxation rates for **1b** sufficiently fast that a local mode contribution with magnitude similar to that for **2a** or **2b** would have little impact on $1/T_1$ for **1b**. The differences in the vibrational modes of **1b** also may make the local mode less effective than for **2a** or **2b**. For diradical **3** the local mode that contributes above about 250 K is the same as for **3_mono** and modulates spin-orbit coupling rather than electron-electron interaction.

At 296 K in sucrose octaacetate T_1 for diradicals **1b**, **2a**, and **2b** are 1.9, 1.5, 1.2 μs, respectively. This temperature is below the glass transition temperature for sucrose octaacetate, so molecular tumbling is too slow to make a significant contribution to the spin-lattice relaxation.[11] Although at lower temperatures $1/T_1$ for **1b** is much faster than for **2a** or **2b**, the substantial contribution of a local mode to the relaxation for **2a** and **2b** is not observed for **1b**, and the relaxation rates for the **1b**, **2a**, and **2b** are more similar near room temperature than at lower temperatures. These T_1 values are substantially shorter than T_1 for **2a_mono** and **1c**, which are 16 and 13 μs. For diradical **3**, the relaxation rates at room temperatures are still about the same as for **3_mono**.

3.5. Molecular Flexibility

To test the suggestion that the faster relaxation rates ($1/T_1$ and $1/T_m$) for **2b** than for **2a** were due to differences in flexibility, optimized geometries and vibrational frequencies were calculated at the unrestricted DFT level (6-31G(d), UB3LYP functional) for model compounds **4a**, syn-**4b**, and anti-**4b**. There are numerous vibrational modes that impact the interspin distance and orientation of the interspin vector. To get a sense of rigidity, a comparison was based on the six lowest-energy modes (Table 4). The antisymmetric out-of-plane breathing mode has a relatively large amplitude of displacement for the nitroxide oxygens and modulates the relative orientations of the two N-O groups. It is an example of a mode that would be expected to modulate dipolar interaction and be effective in spin-lattice relaxation. This mode has a relatively high frequency of 53.5 cm^{-1} in **4a** compared with 6.6 cm^{-1} in syn-**4b**. In anti-**4b** this mode corresponds to a combination of the two lowest frequency modes (15.3 and 22.0 cm^{-1}) (Table 4). The other low-frequency modes have relatively small amplitudes on the N-O atoms and are expected to be much less effective in modulating dipolar interactions. Calculations were not attempted for the much larger calixarenes. Calixarenes **1a** and **1b** possess *tert*-alkylarylnitroxides that are analogous to **2b**, which are expected to contribute to flexibility analogous to **2b**. The saturated aliphatic linkages in the calixarenes provide additional low-energy vibrations that can modulate the spin-spin interaction. These considerations support the proposal that molecular flexibility increases in the order **2a** < **2b** < **1b**.

3.6. Summary of Trends

For diradical **3** with interspin distance about 9 Å, relaxation rates are only slightly faster than for the analogous monoradical **3_mono**, which indicates that the impact of nitroxide-nitroxide interaction on electron spin relaxation extends to relatively short distances compared with the relaxation enhancement by rapidly relaxing metals that extends to tens of angstroms.[14] The inherently slower relaxation rates for the nitroxides makes them less effective in relaxation enhancement. Within the series of diradicals with interspin distances in the range of 5-6 Å, both $1/T_m$ and $1/T_1$ increase in the order **2a** < **2b** < **1b**. This trend does not correlate with trends in the exchange interactions, **1b** ($J/k = 1$ K) < **2b** ($J/k \approx 150$ K) < **2a** ($J/k > 150$ K), which suggests that modulation of the exchange interaction is not the dominant contribution to the relaxation. The trends in $1/T_1$ and $1/T_m$ are therefore attributed to modulation of the dipolar interaction, which is greater for more flexible molecules and for less rigid glasses. The dipolar couplings are small (0.01-0.03 cm^{-1}) relative to thermal and vibrational energies. Although dipolar coupling is not observed in the CW spectra of the tetraradical, relaxation rates are much faster than for the diradicals. EPR transition energies depend strongly on the electron-electron dipolar coupling, so modulation of the multiple dipolar couplings provides an effective spin relaxation pathway. For the tetraradical the presence of multiple spin states may also contribute to relaxation enhancement.

4. Conclusion

Nitroxide-nitroxide interaction at a distance of about 9 Å has little impact on electron spin relaxation in glassy solids. Modulation of the larger electron-electron dipolar interaction at 5-6 Å is a major contributor to both $1/T_1$ and $1/T_m$ for diradicals and a tetraradical. The relaxation enhancement is greater in less rigid nonpolar solvents and greater for the tetraradical than for the diradicals. The largest impact on $1/T_1$ is observed below about 20 K where the direct process dominates. For both monoradicals and diradicals in the low-polarity sucrose octaacetate glass, the Raman process is enhanced relative to that observed in polar hydrogen-bonded glycerol. In glassy solvents at higher temperatures, modulation of the dipolar interaction by a local mode dominates the relaxation for **2a** and **2b** and is solvent-independent. Above the glass softening temperature, modulation of the large dipolar coupling by faster reorientation provides very efficient relaxation pathways and $1/T_m$ and $1/T_1$ increase rapidly. For the tetraradical, the additional energy levels that arise from the multiple exchange interactions, as well as the multiple dipolar interactions, may contribute to enhanced relaxation rates.

Supplementary Material

Refer to Web version on PubMed Central for supplementary material.

Acknowledgment

Financial support of this work by NIH/NIBIB EB002807 (G.R.E. and S.S.E.), NSF/CHE-0414936 (A.R.), and AFOSR/FA9550-04-1-0056 (A.R.) is gratefully acknowledged.

We thank Dr. Sumit Mukherjee for providing samples of tetraradical **1a** and diradical **1b**. Dr. B. M. Sawant prepared **3** in 1983 at the University of Denver.

References and Notes

(1). Budil DE, Lee S, Saxena S, Freed JH. J. Magn. Reson., Ser. A 1996;120:155.

(2). Freed JH. Biol. Magn. Reson 2005;24:239.

(3). Brown, IM. Electron spin echo studies of relaxation processes in molecular solids. In: Kevan, L.; Schwartz, RN., editors. Time Domain Electron Spin Resonance. John Wiley; New York: 1979. p. 195

(4). Salikhov, KM.; Tsvetkov, YD. Electron spin-echo studies of interactions in solids. In: Kevan, L.; Schwartz, RN., editors. Time Domain Electron Spin Resonance. Wiley; New York: 1979. p. 232

(5). Hubbell WL, Cafiso DS, Altenbach C. Nat. Struct. Biol 2000;7:735. [PubMed: 10966640]

(6). Berliner, LJ.; Eaton, GR.; Eaton, SS., editors. Distance Measurements in Biological Systems by EPR. Vol. 19. Kluwer; New York: 2000. p. 614

(7). Jeschke G. ChemPhysChem 2002;3:927. [PubMed: 12503132]

(8). Winalski CS, Shortkroff S, Mulkern RV, Schneider E, Rosen GM. Magn. Reson. Med 2002;48:965. [PubMed: 12465105]

(9). Armstrong BD, Han S. J. Chem. Phys 2007;127:104508/1. [PubMed: 17867762]

(10). Sato H, Kathirvelu V, Fielding AJ, Bottle SE, Blinco JP, Micallef AS, Eaton SS, Eaton GR. Mol. Phys 2007;105:2137.

(11). Owenius R, Terry GE, Williams MJ, Eaton SS, Eaton GR. J. Phys. Chem. B 2004;108:9475.

(12). Eaton SS, Eaton GR. Biol. Magn. Reson 2000;19:29.

(13). Kulikov AV, Likhtenshtein GI. Adv. Mol. Relax. Interact. Processes 1977;10:47.

(14). Eaton SS, Eaton GR. Biol. Magn. Reson 2000;19:347.

(15). Rajca A, Mukherjee S, Pink M, Rajca S. J. Am. Chem. Soc 2006;128:13497. [PubMed: 17031963]

(16). Rajca A, Takahashi M, Pink M, Spagnol G, Rajca S. J. Am. Chem. Soc 2007;129:10159. [PubMed: 17655296]

(17). Nakajima A. Bull. Chem. Soc. Jpn 1973;46:1129.

(18). Michon J, Michon P, Rassat A. Nouv. J. Chim 1978;2:619.

(19). Eaton SS, More KM, Sawant BM, Eaton GR. J. Am. Chem. Soc 1983;105:6560.

(20). Spagnol G, Shiraishi K, Rajca S, Rajca A. Chem. Commun 2005:5047.

(21). Sawant BM, Eaton GR, Eaton SS. J. Magn. Reson 1981;45:162.

(22). Spagnol G, Rajca A, Rajca S. J. Org. Chem 2007;72:1867. [PubMed: 17266379]

(23). Hurrey ML, Wallen SL. Langmuir 2006;22:7324. [PubMed: 16893233]

(24). Brinkmann M, Andre JJ. J. Mater. Chem 1999;9:1511.

(25). Quine RW, Eaton SS, Eaton GR. Rev. Sci. Instrum 1992;63:4251.

(26). Hanson GR, Gates KE, Noble CJ, Griffin M, Mitchell A, Benson S. J. Inorg. Biochem 2004;98:903. [PubMed: 15134936]

(27). Eaton SS, Eaton GR. J. Magn. Reson., Ser. A 1995;117:62.

(28). Du J-L, Eaton GR, Eaton SS. J. Magn. Reson., Ser. A 1995;115:213.

(29). Sato H, Filas BA, Eaton SS, Eaton GR, Romanyukha AA, Hayes R, Rossi AM. Radiat. Meas 2007;42:997.

(30). Borgia GC, Brown RJS, Fantazzini P. J. Magn. Res 1998;132:65.

(31). Borgia GC, Brown RJS, Fantazzini P. J. Magn. Res 2000;147:273.

(32). Zecevic A, Eaton GR, Eaton SS, Lindgren M. Mol. Phys 1998;95:1255.

(33). Zhou Y, Mitri R, Eaton GR, Eaton SS. Curr. Top. Biophys 1999;23:63.

(34). Frisch, MJ.; Trucks, GW.; Schlegel, HB.; Scuseria, GE.; Robb, MA.; Cheeseman, JR.; Montgomery, JA., Jr.; Vreven, T.; Kudin, KN.; Burant, JC.; Millam, JM.; Iyengar, SS.; Tomasi, J.; Barone, V.; Mennucci, B.; Cossi, M.; Scalmani, G.; Rega, N.; Petersson, GA.; Nakatsuji, H.; Hada, M.; Ehara, M.; Toyota, K.; Fukuda, R.; Hasegawa, J.; Ishida, M.; Nakajima, T.; Honda, Y.; Kitao, O.; Nakai, H.; Klene, M.; Li, X.; Knox, JE.; Hratchian, HP.; Cross, JB.; Bakken, V.; Adamo, C.; Jaramillo, J.; Gomperts, R.; Stratmann, RE.; Yazyev, O.; Austin, AJ.; Cammi, R.; Pomelli, C.; Ochterski, JW.; Ayala, PY.; Morokuma, K.; Voth, GA.; Salvador, P.; Dannenberg, JJ.; Zakrzewski, VG.; Dapprich, S.; Daniels, AD.; Strain, MC.; Farkas, O.; Malick, DK.; Rabuck, AD.; Raghavachari, K.; Foresman, JB.; Ortiz, JV.; Cui, Q.; Baboul, AG.; Clifford, S.; Cioslowski, J.; Stefanov, BB.; Liu, G.; Liashenko, A.; Piskorz, P.; Komaromi, I.; Martin, RL.; Fox, DJ.; Keith, T.; Al-Laham, MA.; Peng, CY.; Nanayakkara, A.; Challacombe, M.; Gill, PMW.; Johnson, B.; Chen, W.; Wong, MW.; Gonzalez, C.; Pople, JA. Gaussian 03, revision C.02. Gaussian, Inc.; Wallingford, CT: 2004.

(35). Lajzerowicz-Bonneteau, J. Molecular structure of nitroxides. In: Berliner, LJ., editor. Spin Labeling: Theory and Applications. Academic Press; New York: 1975. p. 239

(36). Dzuba SA. Phys. Lett. A 1996;213:77.

(37). Dzuba SA. Spectrochim. Acta, Part A 2000;56:227.

(38). Freed, JH. Theory of slow tumbling ESR spectra of nitroxides. In: Berliner, LJ., editor. Spin Labeling: Theory and Applications. Academic Press; New York: 1976. p. 53

(39). Du JL, More KM, Eaton SS, Eaton GR. Isr. J. Chem 1992;32:351.

(40). Tsvetkov YD, Dzuba SA. Appl. Magn. Reson 1990;1:179.

(41). Nakagawa K, Candelaria MB, Chik WWC, Eaton SS, Eaton GR. J. Magn. Reson 1992;98:81.

(42). Abragam, A.; Bleaney, B. Electron Paramagnetic Resonance of Transition Ions. Oxford University Press; Oxford: 1970. Spin-spin interactions; p. 552

(43). Zhou Y, Bowler BE, Eaton GR, Eaton SS. J. Magn. Reson 1999;139:165. [PubMed: 10388595]

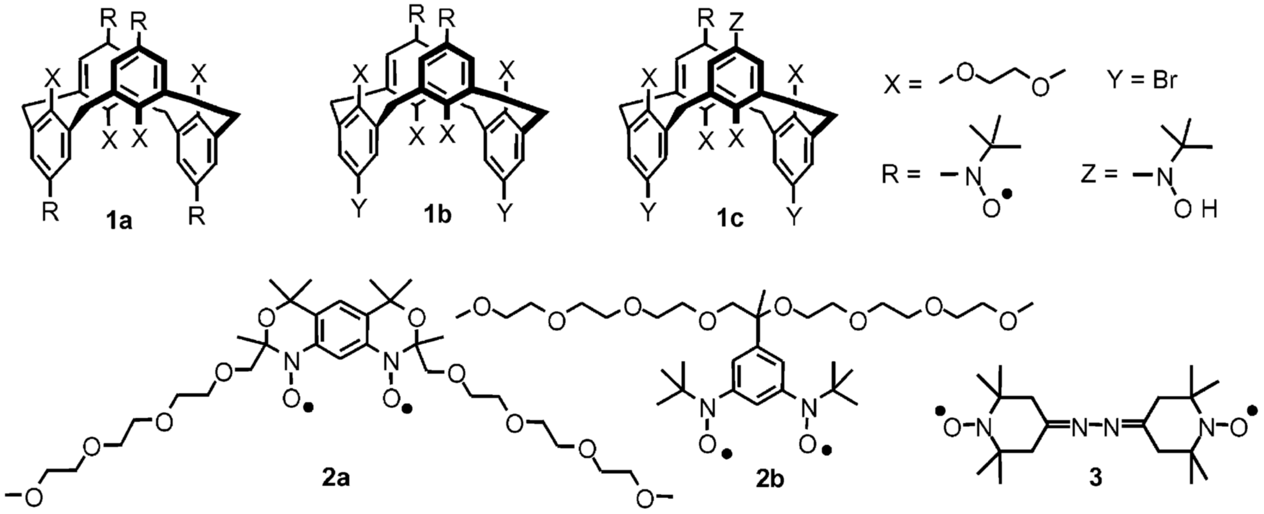

Figure 1.

Structures of nitroxide tetraradical **1a**, diradical **1b**, and monoradical **1c** derivatives of 1,3-alternate calix[4]arene, pegylated nitroxide diradicals **2a** and **2b**, and azine diradical **3**. The small amount of monoradical that is present in samples of **2a** is designated as **2a_mono**. monoradical formed by partial reduction of **3** is designated as **3_mono**.

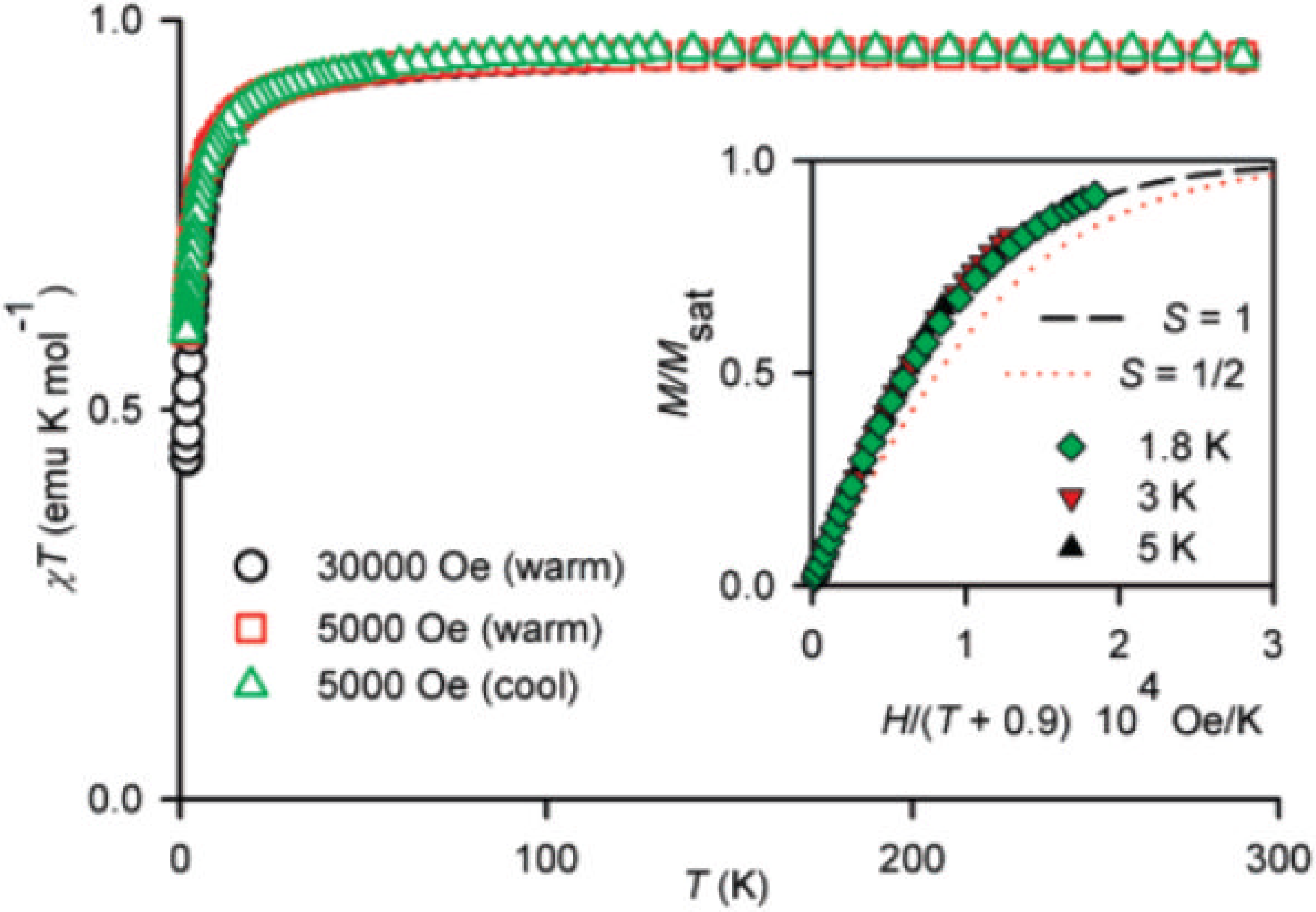

Figure 2.

SQUID magnetometry for solid diradical **2a**. The main plot corresponds to χT vs T in both cooling and warming modes, with $\chi T \approx 0.96$ emu K mol^{-1} in the high-temperature range. The inset plot corresponds to M/M_{sat} vs $H/(T - \theta)$, with dotted and dashed lines showing plots of Brillouin functions with $S = ½$ and $S = 1$, respectively; numerical fits to the Brillouin functions with $\theta = -0.9$ K give $S \approx 1.0$ at 1.8, 3, and 5 K.

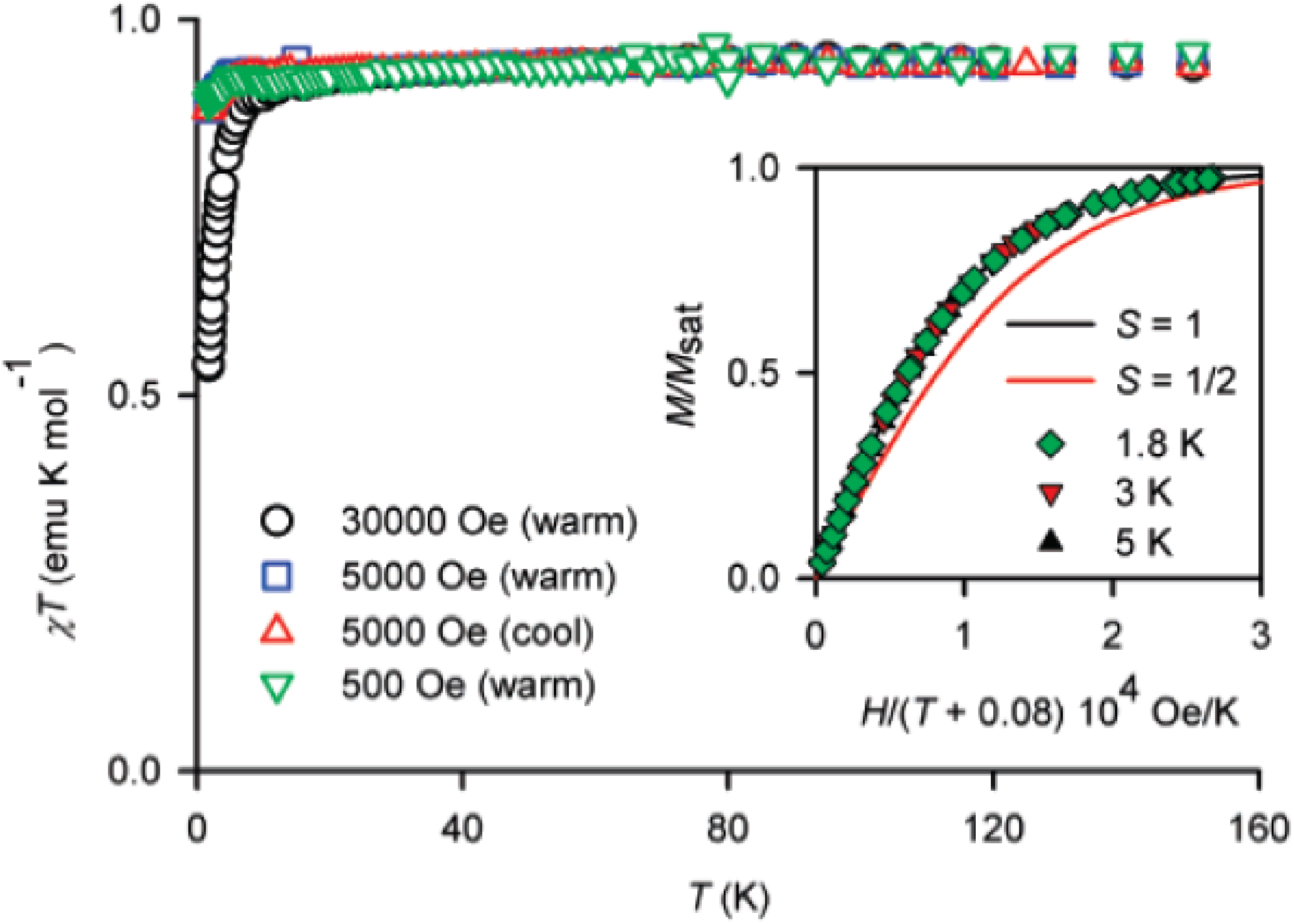

Figure 3.

SQUID magnetometry for ~10 mM diradical **2a** in EtOH/H_2O (2:1). The main plot corresponds to χT vs T in both cooling and warming modes, with $\chi T \approx 0.94$ emu K mol^{-1} in the high-temperature range. The inset plot corresponds to M/M_{sat} vs $H/(T - \theta)$, with solid lines showing plots of Brillouin functions with $S = ½$ and $S = 1$; numerical fits to the Brillouin functions with $\theta = -0.08$ K give $S = 1.00$ and $M_{sat} \approx 0.93\ \mu_B$ (per nitroxide site) at 1.8, 3, and 5 K.

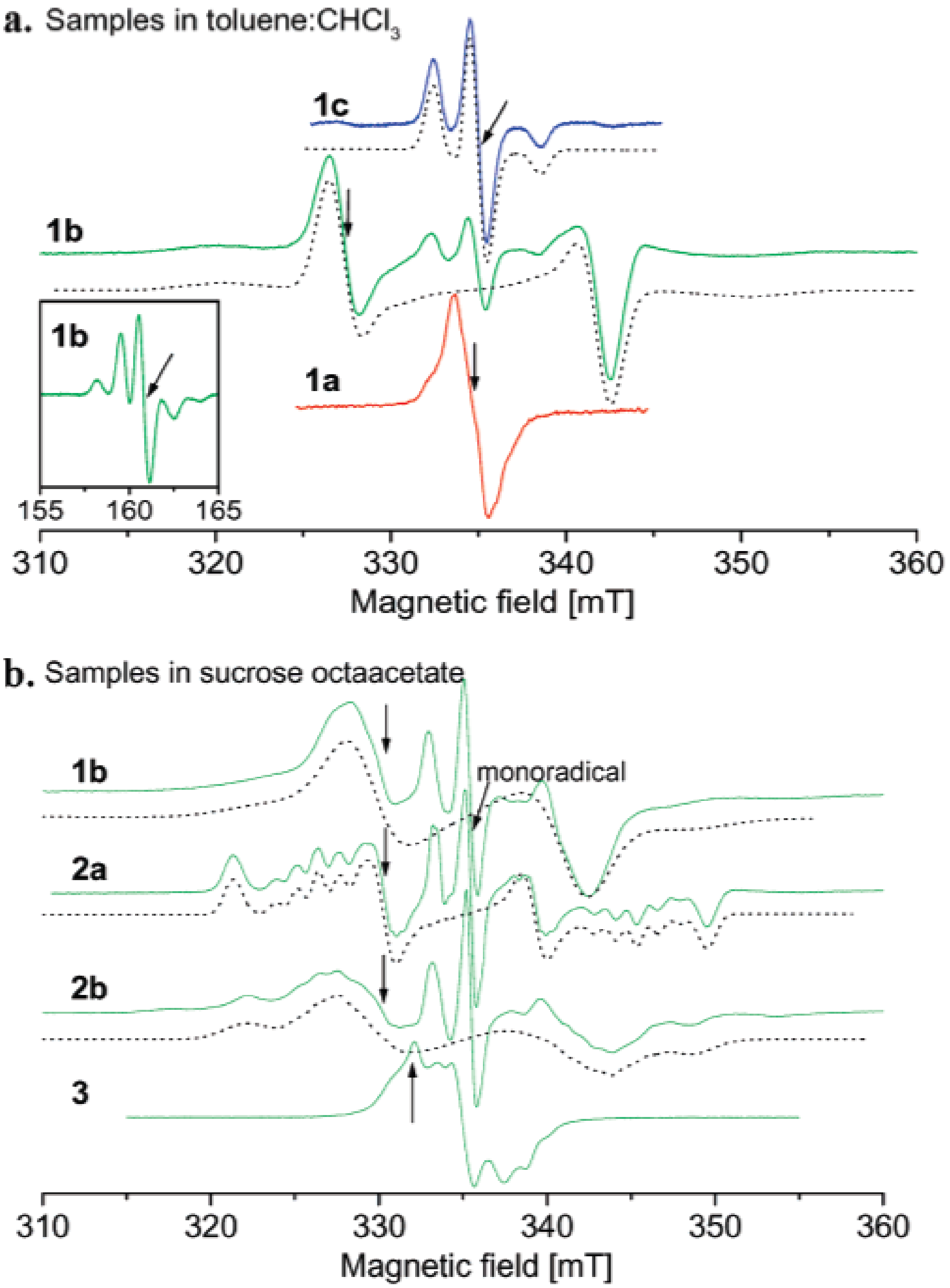

Figure 4.

(a) X-band CW spectra in toluene/CHCl$_3$ mixture (4:1) of nitroxide tetraradical **1a** at 50 K, diradical **1b** at 50 K, and monoradical **1c** at 60 K. (b) CW spectra at 294 K in sucrose octaacetate of diradicals **1b**, **2a**, **2b**, and **3**. The arrows mark the positions in the spectra where the measurements of T_1 and T_m were performed. Simulated spectra are shown as dashed lines.

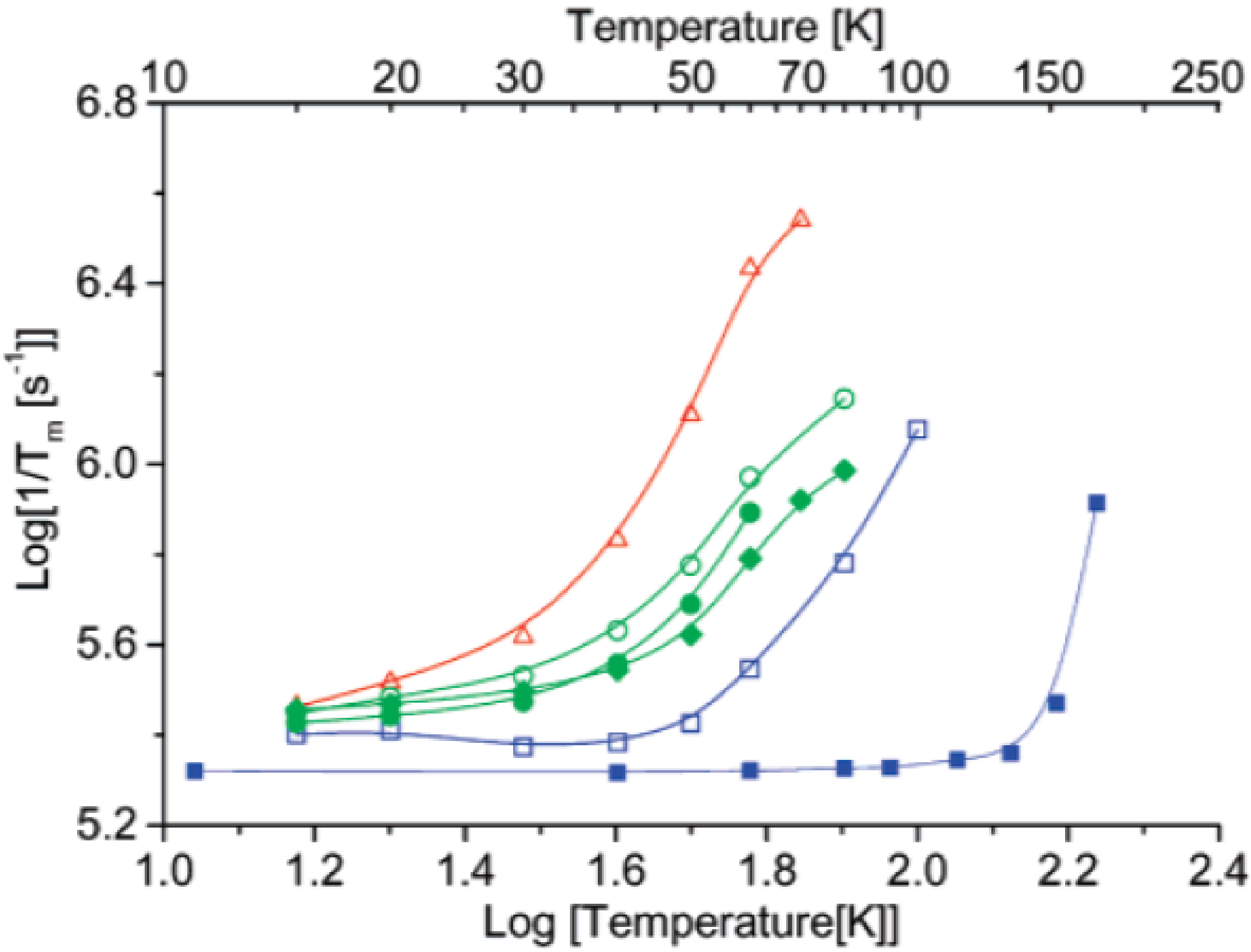

Figure 5.

Temperature dependence of 1/T_m at X-band: (red open triangles) tetraradical **1a**, (green open circles) diradical **1b**, (green solid diamonds) diradical **2a**, (green solid circles) diradical **2b**, and (blue open squares) monoradical **1c**, in 4:1 toluene/$CHCl_3$, and (blue solid squares) Fremy's salt in water/glycerol. Relaxation rates were estimated by a single-exponential fit. Lines connect the data points. The positions in the CW spectra at which relaxation rates were measured are shown in Figure 4.

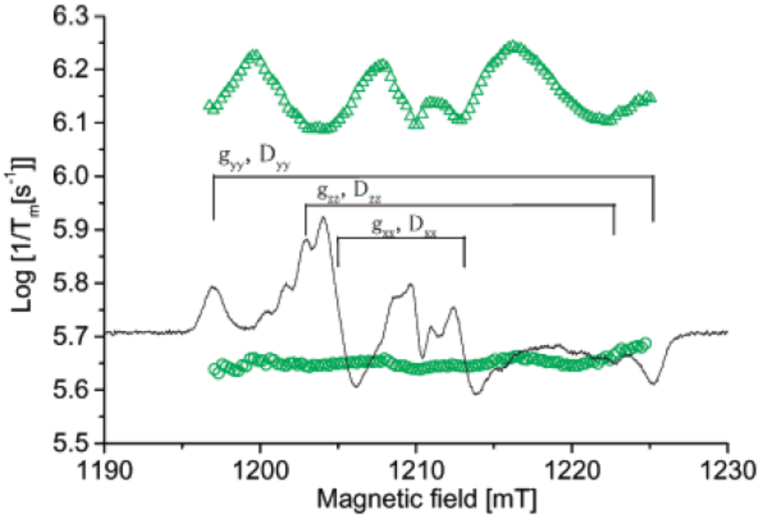

Figure 6.

Dependence of $1/T_m$ for diradical **2a** on position in the spectrum at 86 K at Q-band in (green circles) glycerol and (green triangles) sucrose octaacetate. Relaxation rates were estimated by a single-exponential fit. The plots of relaxation rates are superimposed on the Q-band CW spectrum in sucrose octaacetate.

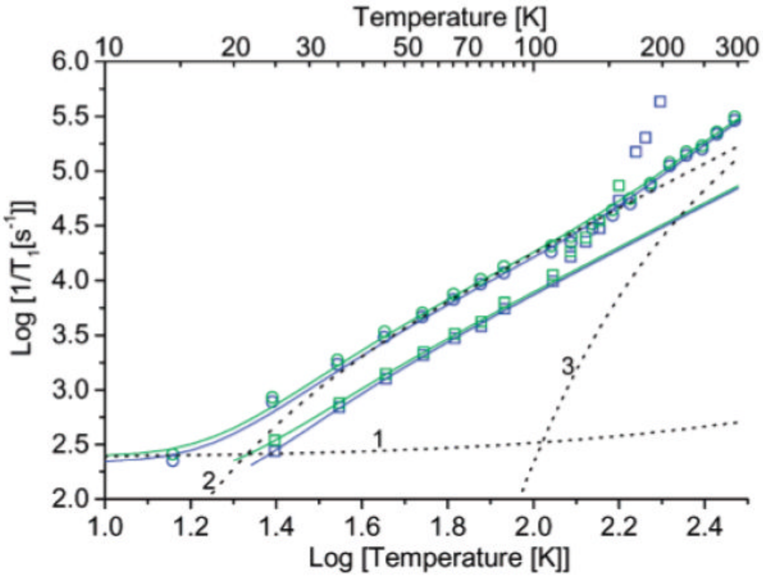

Figure 7.

Comparison of the temperature dependence of $1/T_1$ in 4:1 toluene/$CHCl_3$ for (green squares) **3** and (blue squares) **3_mono** and in sucrose octaacetate for (green circles) **3** and (blue circles) **3a_mono**. The dashed lines 1, 2, and 3 are the contributions to the relaxation of **3** in sucrose octaacetate calculated for the direct, Raman, and local mode processes, respectively.

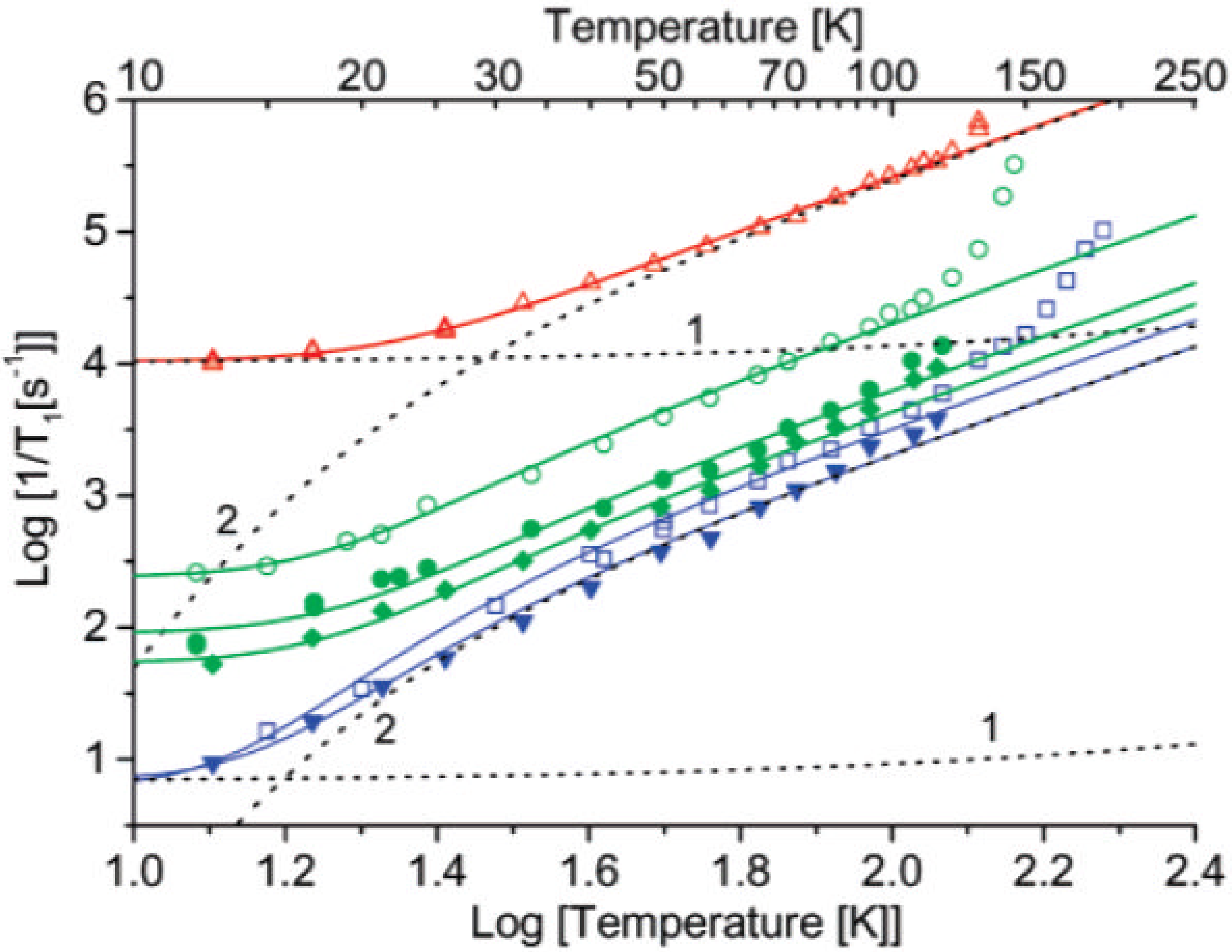

Figure 8.

Spin lattice relaxation $1/T_1$ in 4:1 toluene/$CHCl_3$ at X-band: (red triangles) tetraradical **1a**, diradicals ((green open circles) **1b**, (green solid circles) **2b**, and (green diamonds) **2a**) and monoradicals (blue squares) **1c** and (blue triangles) **2a_mono**) measured by saturation recovery (SR). The positions in the spectra where the data were recorded are marked in Figure 4b. The dashed lines 1 and 2 are the contributions to the relaxation of **1a** and **1c** calculated for the direct and Raman processes, respectively. The solid lines are calculated using the fit parameters listed in Table 3 and Supporting Information Table S1.

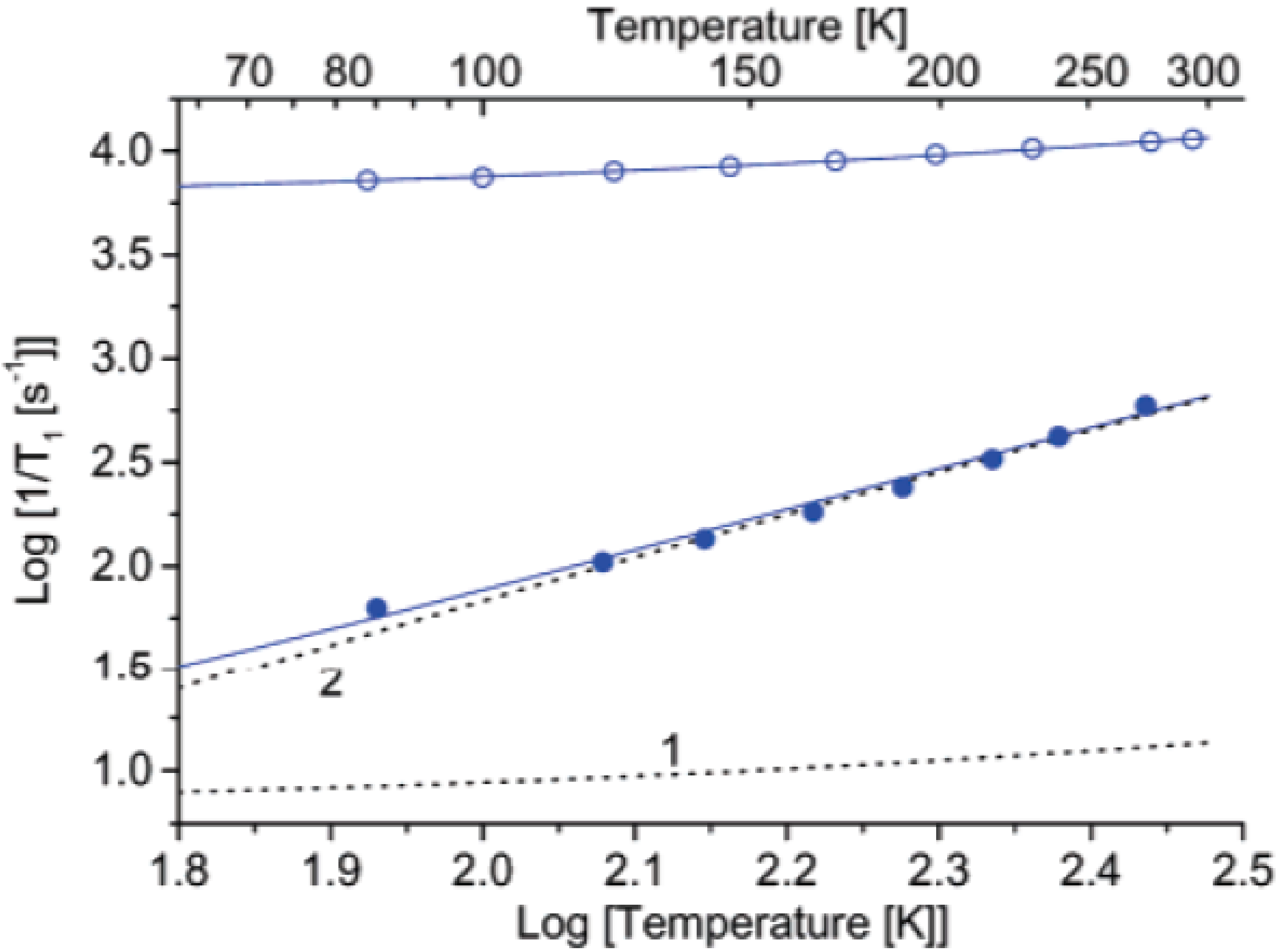

Figure 9.

Temperature dependence of 1/T_1 for (blue open circles) 44 mM BDPA and (blue solid circles) 1.1 or 0.1 mM BDPA in sucrose octaacetate measured by SR at Q-band. The dashed lines 1 and 2 are the contributions to relaxation calculated for the direct and Raman processes, respectively.

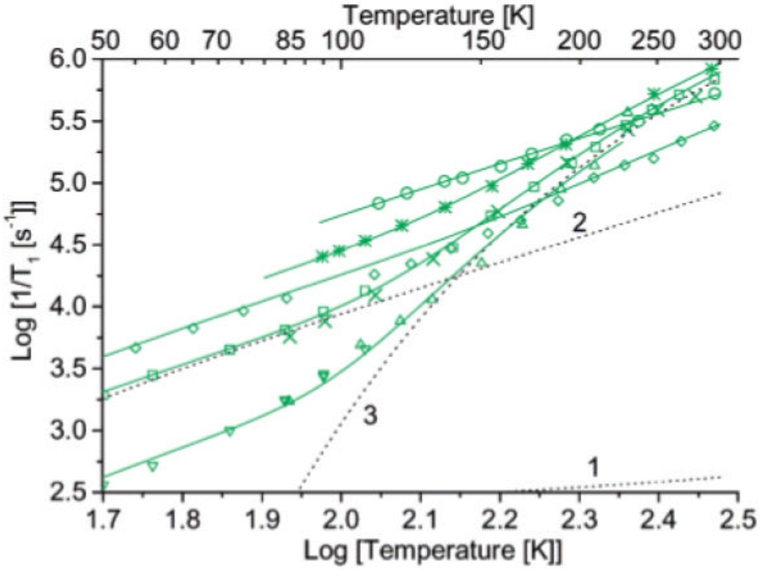

Figure 10.

Temperature dependence of $1/T_1$ for diradicals in sucrose octaacetate: (green circles) **1b** by SR at X-band, (green squares) **2a** by SR at X-band, (green crosses) **2a** by inversion recovery at Q-band, (green asterisks) **2b** by inversion recovery at X-band, (green diamonds) **3** by saturation recovery (SR) at X-band. Temperature dependence in glycerol: (green down triangles) **2a** by SR at X-band and (green up triangles) **2a** by SR at Q-band. The positions in the spectra where the data were recorded are marked in Figure 4b. The solid lines are fit lines calculated with the parameters in Table 3. The dashed lines 1, 2, and 3 are the contributions to relaxation for **2a** in sucrose octaacetate calculated for the direct, Raman, and local mode processes, respectively.

TABLE 1

Interspin Distances and Exchange Interactions

compd	S	*r* (Å)	|*J*/*k*| (K)
1a	2, 1[a]	5-6[b]	~1[a]
1b	1	5-6[c]	~1[a]
2a	1	5-6[d]	>150
2b	1	6.0[e]	~150
3	1	8-9[f]	>0.1

[a] Determined by magnetic susceptibility (ref 15).

[b] Calculated from the X-ray crystal structure (ref 15).

[c] Estimated interspin distances calculated from the dipolar splitting, the X-ray crystal structure, and the relative intensity of the half-field transitions are 5.7, 5-6, and 5.7 Å, respectively (ref 15).

[d] Estimated interspin distances calculated from the dipolar splittings and average of nitroxyl N-N and O-O distances in the crystal structure of **4a** (ref 16) (which does not account for spin delocalization into the aromatic ring) are 5.8 and 4.8 Å, respectively.

[e] The interspin distance calculated from the dipolar splitting is 6.0 Å. For the two isomers the average of N-N and O-O distances in the structures calculated by DFT are 4.9 and 6.2 Å, respectively.

[f] Determined from dipolar splittings (ref 18), single-crystal EPR (ref 17), and the relative intensity of the half-field transitions (ref 19).

TABLE 2
Dipolar Couplings and Line Widths from CW Spectra

sample	**temp (K)**	**$\lvert D_{xx}\rvert, \lvert D_{yy}\rvert, \lvert D_{zz}\rvert$ (mT)**[a]	**line widths (mT) (x, y, z)**
toluene/$CHCl_3$ (4:1)			
1b (di)	50	15.1, 15.1, 30.2	0.9, 0.9, 0.9
1c (mono)	60		0.35, 0.4, 0.55
2a (di)	70	8.13, 28.0, 19.9	0.6, 0.5, 0.45
2b (di)	50	11.2,[b] 26.1, 14.1[b]	2.7,[c] 1.0, 0.5
sucrose octaacetate			
1b (di)	294	12.5, 12.5, 25.0	2.5, 1.5, 2.0
2a (di)	294	9.2, 28.2, 19.0	0.7, 0.5, 0.45
2a (di)[d]	86	8.4, 28.2, 19.8	0.7, 0.5, 0.53
2b (di)	294	10.5,[b]26.4, 15.9[b]	2.7,[c]1.5, 0.6

[a] Components of the zero-field splitting tensor along the axes of the nitroxide radical.

[b] Due to broad lines the values of D_{XX} and D_{ZZ} are uncertainbut were constrained to satisfy the relationship that $D_{XX} + D_{YY} + D_{ZZ} = 0$.

[c] The spectra are relatively insensitive to this parameter, so the uncertainty is greater.

[d] Based on the Q-band CW spectrum.

TABLE 3

Fit Parameters for Temperature Dependence of $1/T_1$

structure	solvent	direct[a]	Raman[b]	local mode[c]
1a (tetra)	4:1 toluene/$CHCl_3$	37	184×10^4	
1b (di)	4:1 toluene/$CHCl_3$	0.88	14×10^4	
2a (di)	4:1 toluene/$CHCl_3$	0.2	3.1×10^4	
2b (di)	4:1 toluene/$CHCl_3$	0.33	4.6×10^4	
3	4:1 toluene/$CHCl_3$	[d]	5.7×10^4	
1c (mono)	4:1 toluene/$CHCl_3$	0.02	2.4×10^4	
2a_mono	4:1 toluene/$CHCl_3$	0.02	1.5×10^4	
3_mono	4:1 toluene/$CHCl_3$	[d]	5.4×10^4	
1b (di)	sucrose octaacetate	[e]	41×10^4	
2a (di)	sucrose octaacetate	[e]	6.5×10^4	15×10^6
2b (di)	sucrose octaacetate	[e]	21×10^4	14×10^6
3	sucrose octaacetate	[e]	13×10^4	2.8×10^6
2a_mono	sucrose octaacetate	[e]	3.2×10^4	0.64×10^6
3_mono	sucrose octaacetate	[e]	12×10^4	2.8×10^6
2a (di)	glycerol	<0.02	1.5×10^4	13×10^6

[a] Direct process from dipolar interaction; $1/T_1$)$a(T + 270)$.

[b] Raman process with Debye temperature fixed at 100 K.

[c] Local mode with a fixed vibration energy of 950 K.

[d] SR data were recorded only above 25 K.

[e] SR data in sucrose octaacetate were recorded primarily at temperatures where the contribution from the direct process was not significant.

TABLE 4

Lowest Vibrational Frequencies for Triplet States of Model Nitroxide Diradicals Calculated at the UB3LYP/ 6-31G(d) Level

W Animations of selected vibrational modes of W 4a, W syn-4b, and W anti-4b in JMol format are available.

Low Frequency Vibrations (cm^{-1})		
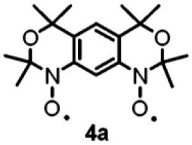 **4a**	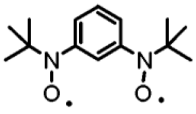 syn-**4b**	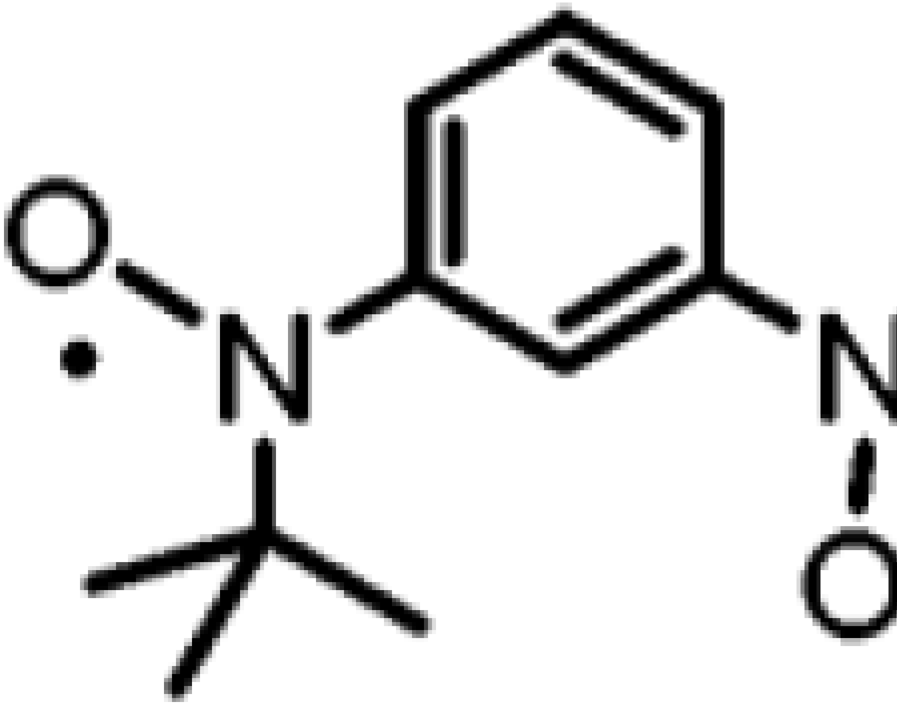 anti-**4b**
29.7	6.6*	15.3*
31.2	10.5	22.0*
53.5*	43.9	41.0
78.2	68.1	68.7
127.2	84.0	76.1
127.9	105.0	92.5

*Antisymmetric out-of-plane breathing mode, which is an example of a vibration that modulates electron-electron dipolar coupling.

Supporting Information

Impact of the modulation of electron-electron dipolar interaction on electron spin relaxation of nitroxide diradicals and tetraradical in glassy solvents between 10 and 300 K

Hideo Sato, Velavan Kathirvelu, Gaëlle Spagnol, Suchada Rajca, Andrzej Rajca, Sandra S. Eaton, and Gareth R. Eaton

Department of Chemistry and Biochemistry, University of Denver, Denver, CO 80208-2436 and Department of Chemistry, University of Nebraska, Lincoln, NE 68588-0304

Table of Content

Preparation of Calix[4]arene Nitroxide Monoradical 1c.

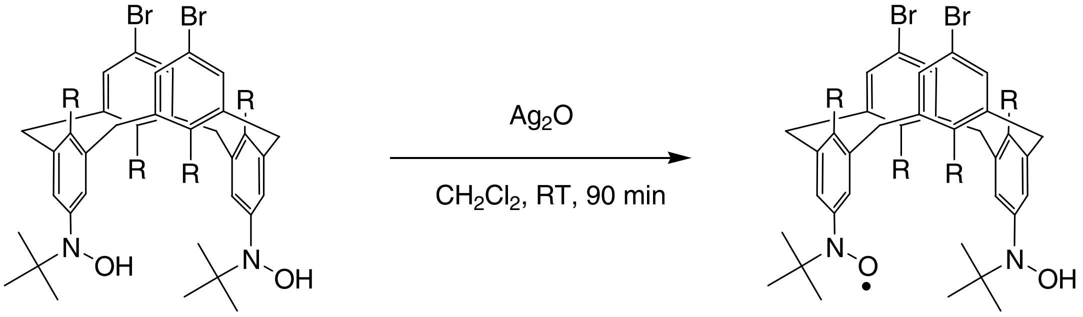

R = $OCH_2CH_2OCH_3$

A solution of the dihydroxylamine (34.9 mg, 0.0353 mmol, 1 equiv) in degassed chloroform (3.0 mL) was added onto freshly prepared silver oxide (328 mg, 1.41 mmol, 40 equiv). The reaction mixture, protected from light, was stirred vigorously at room temperature for ~90 min. The crude mixture was centrifuged and the supernatant liquid was filtered through a 0.45-µm filter (Fisher) to remove silver oxide. Concentration under reduced pressure gave a dark orange solid (33.1 mg), which was purified by flash chromatography (TLC-grade silica gel, gradient hexane/ether, 7:3 to 5:5). The silica pad was kept at low temperature, between –5 and 0 °C, by a sleeve filled with EtOH cooled with dry ice. The target material was collected as a pale orange pinkish band (1.3 mg). The EPR spectrum of **1c** in glassy 4:1 toluene:$CHCl_3$ is shown in Figure 5a, top trace. The g and A values are included in Table S1.

Table S1

g values and Nitrogen Hyperfine Couplings

Sample	Temp (K)	g_{xx}, g_{yy}, g_{zz}	A_{zz} (G)[a]
Toluene: $CHCl_3$ (4:1)			
1b (di)	50	2.0093, 2.0058, 2.0026	15.4[b]
1c (mono)	60	2.0091, 2.0056, 2.0024	30.8
2a (di)	70	2.0089, 2.0055, 2.0024	12.5
2b (di)	50	2.0091, 2.0060, 2.0025	12
sucrose octaacetate			
1b (di)	294	2.0080, 2.0043, 2.0022	15.4[b]
2a (di)	294	2.0089, 2.0054, 2.0025	12.5
2a (di)[e]	86	2.0087, 2.0050, 2.0021	12.7
2b (di)	294	2.0089, 2.0054, 2.0025	12.5

[a] Hyperfine values A_{xx} and A_{yy} were not resolved but were assumed to be in the range of 2 to 3 G, which is half the value for the monoradical.

[b] A_{zz} was not resolved in the spectrum and was assumed to be half the value for the monoradical.

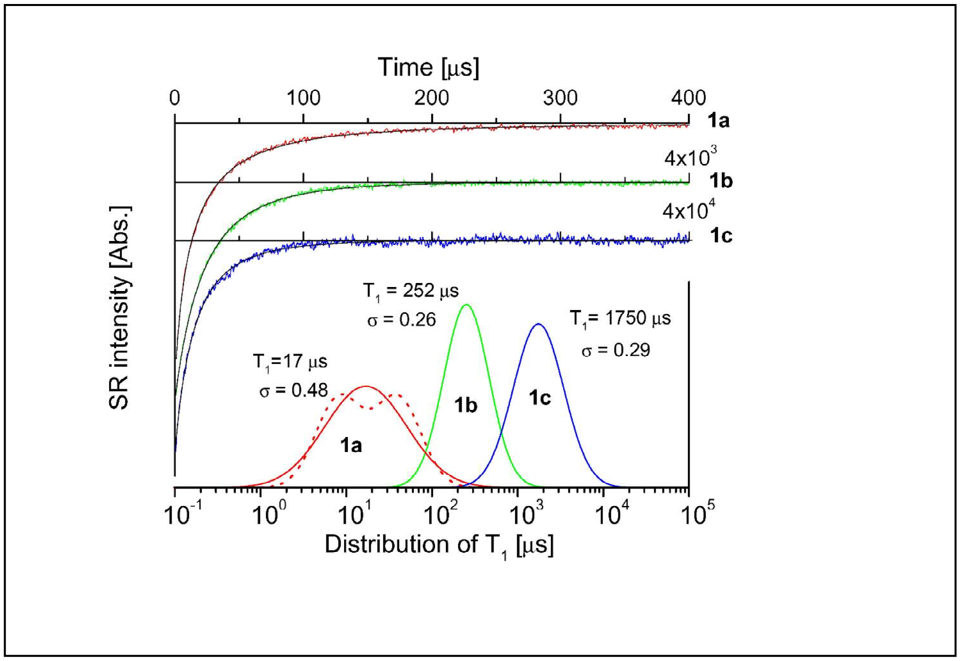

Figure S1. Saturation recovery curves and fit line calculated for a log-normal distributions of T_1 for tetraradical **1a**, diradical **1b** and monoradical **1c** in 4:1 toluene:$CHCl_3$ at 50 K. The distributions, distribution widths and values of T_1 are shown in the lower part of the figure. An alternate modeling of the data for tetraradical **1a** as the sum of two distributions is also shown.

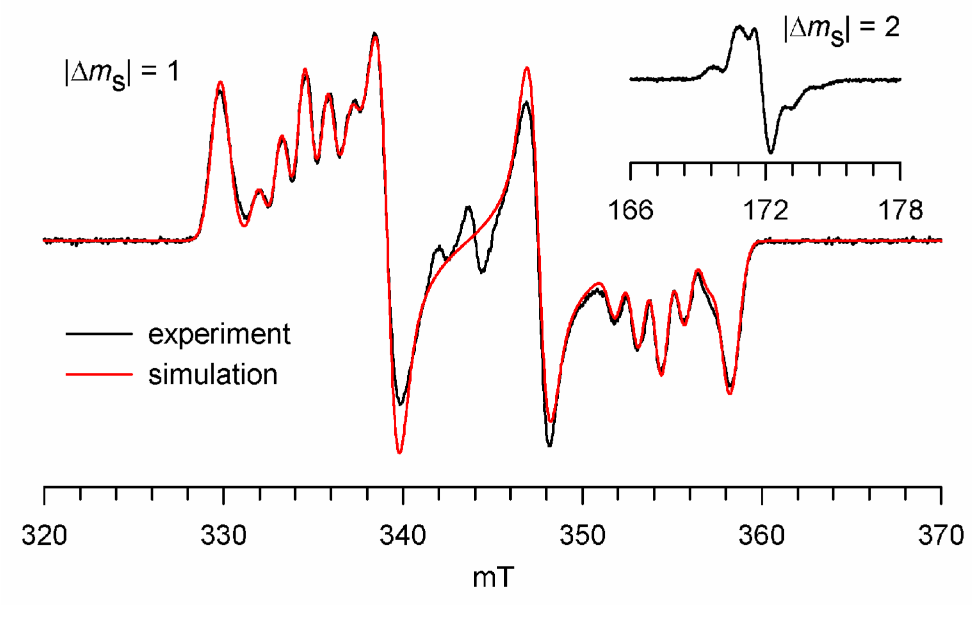

Figure S2. EPR (X-Band, 9.6545 GHz) spectrum of 0.7 mM nitroxide diradical **2a** in ethanol/water (2 : 1) at 140 K. The spectral simulation of the $|\Delta m_s| = 1$ region is shown as red trace. The fitting parameters for the spectral simulation to the $S = 1$ state are: $|D/hc| = 1.328 \times 10^{-2}$ cm^{-1}, $|E/hc| = 1.75 \times 10^{-3}$ cm^{-1}, $|A_{yy}/2hc| = 1.20 \times 10^{-3}$ cm^{-1}, $g_x = 2.0086$, $g_y = 2.0022$, $g_z = 2.0051$, Gaussian line ($L_x = 10$ G, $L_y = 7.5$ G, $L_z = 10$ G). The center lines correspond to an $S = ½$ (monoradical) impurity. The molecular *x*-, *y*-, and *z*-axes for this spectral simulation are set to correspond to the increasing values of the principal components for the spin-spin magnetic dipole tensor, as implemented in WINEPR SimFonia 1.25.

a.

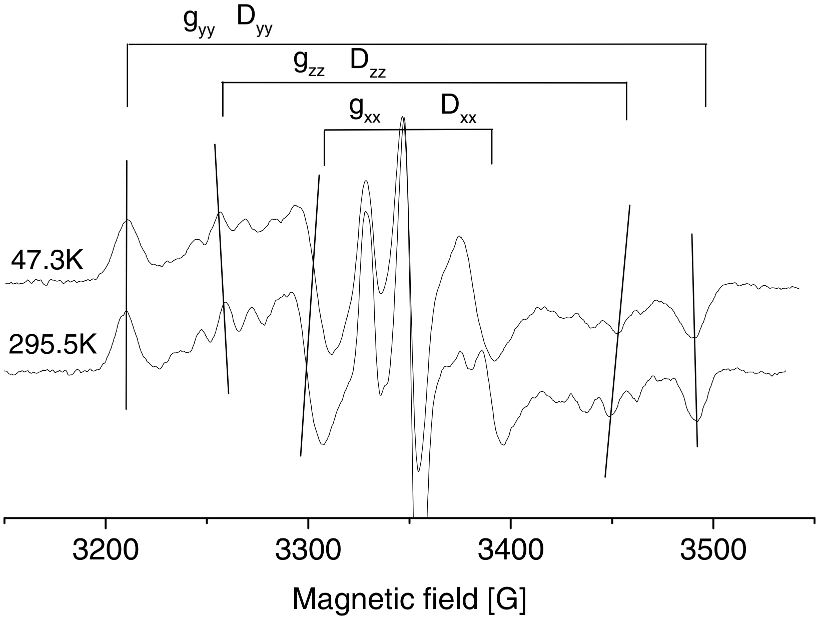

b.

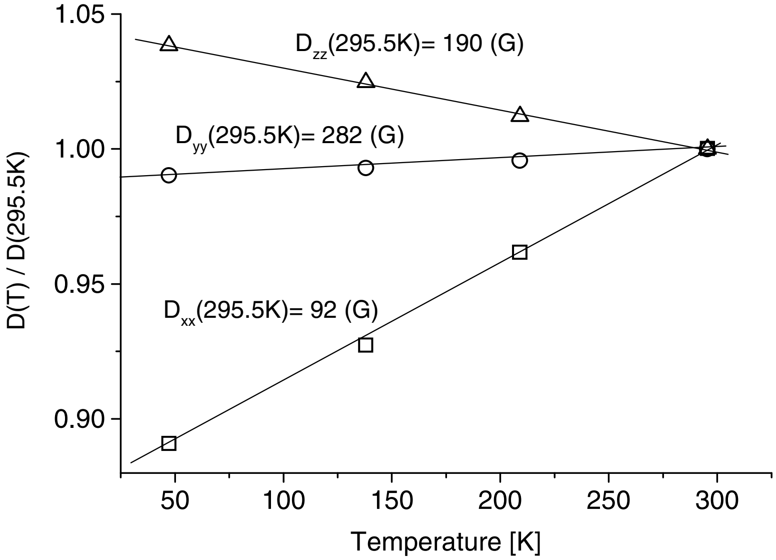

Figure S3. (a) Temperature dependence of X-band CW spectra of diradical **2a** in sucrose octaacetate; (b) temperature dependence of dipolar couplings D_{xx}, D_{yy} and D_{zz} normalized to the values at 295.5 K.

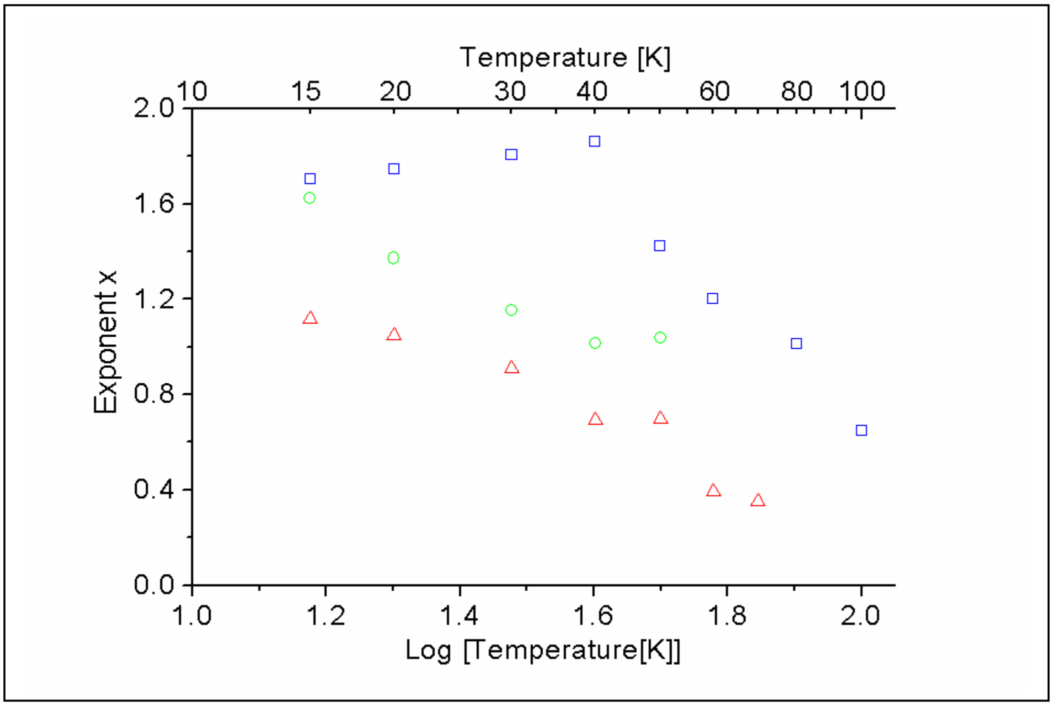

Figure S4: Temperature dependence of exponent x (Equation [3] for spin echo decays for (△) tetraradical **1a**, (O) diradical **1b**, and (□) monoradical **1c** in 4:1 toluene:$CHCl_3$.

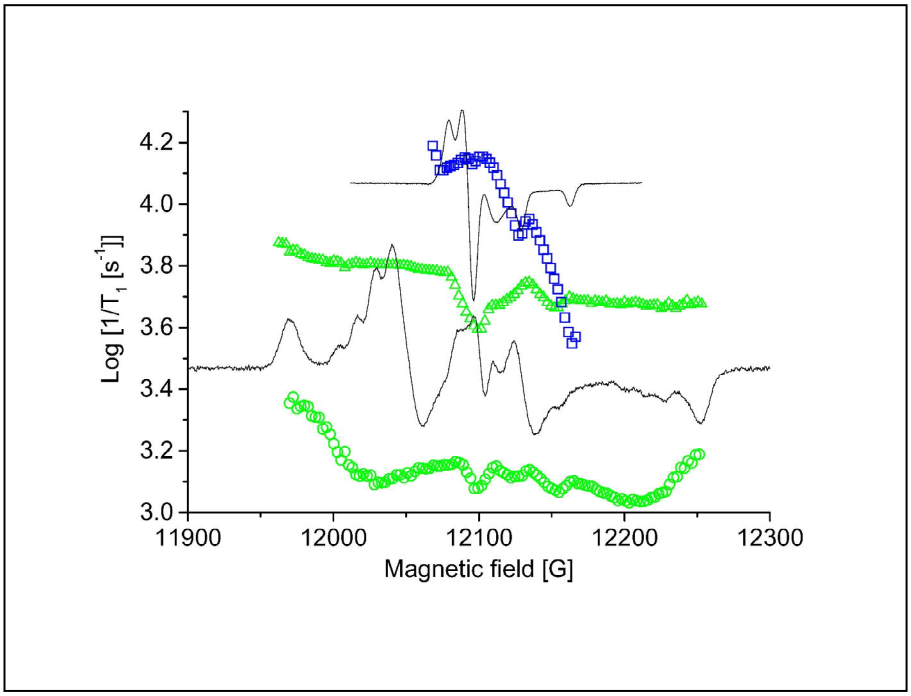

Figure S5. Dependence of $1/T_1$ on position in Q-band spectra at 86 K: (□) tempone in sucrose octaacetate, (○) diradical **2a** in glycerol, and (△) diradical **2a** in sucrose octaacetate. Relaxation rates were estimated by a single exponential fit. The relaxation rates are superimposed on CW spectra in sucrose octaacetate.

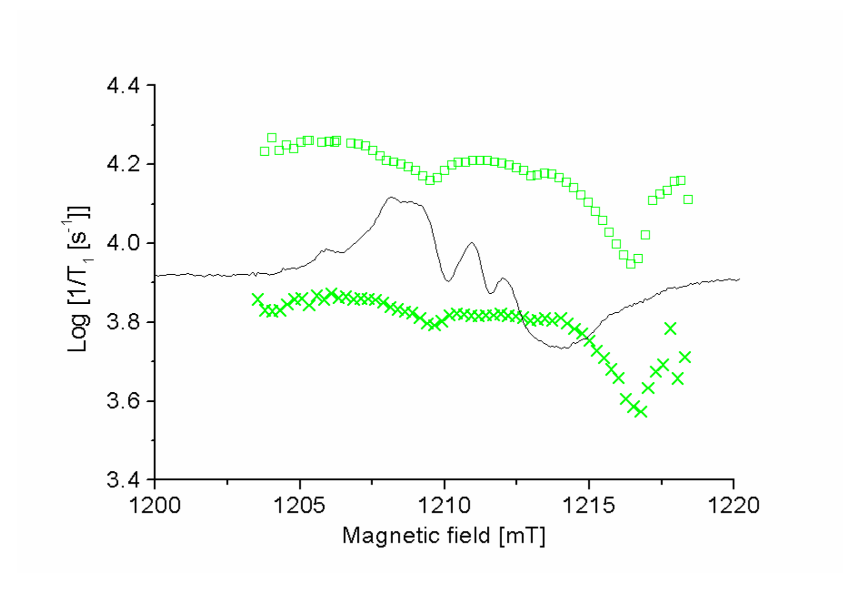

Figure S6. Dependence of $1/T_1$ on position for diradical **3** in Q-band spectra at 86 K: (□) in sucrose octaacetate and (x) in 4:1 toluene:$CHCl_3$. Relaxation rates were estimated by a single exponential fit. The relaxation rates are superimposed on CW spectra in sucrose octaacetate.

Discussion of Figures S5 and S6.

Dependence of $1/T_1$ on Position in the CW Spectra. To enhance orientation selectivity these experiments were performed primarily at Q-band. The variation with position in the spectrum of $1/T_1$ for nitroxide radicals has been reported at X-band.[1] The maximum rates, which are observed near g_{xx} and g_{yy}, are about a factor of 4 faster than the minimum rates that are observed at g_{zz}. This dependence is clearly resolved at Q-band for tempone in sucrose octaacetate at 86 K (Figure S5) where the Raman process is the dominant contribution to $1/T_1$. The rates are similar at X- band and Q-band as expected for the Raman process This orientation dependence, which persists with increasing temperature until the tumbling process dominates, is due to the orientation dependence of spin-orbit coupling or of vibrations.[1]

The relaxation rates for diradical **2a** in the relatively rigid glycerol glass at 86 K at Q-band are shown in Figure S5. The variation with position in the spectrum is only about a factor of 2, which is substantially smaller than for mono-nitroxides. Rates are faster toward the extremes of the spectrum, which is along the g_{yy} axis of the nitroxide and slower near the g_{zz} axis, as in the monoradical. The slightly slower relaxation at the monoradical position (the center of the spectrum) is due to the overlap of the monoradical contribution (**2a_mono**). In sucrose octaacetate, the relaxation for **2a** is faster than in glycerol due to a larger contribution from modulation of the dipole-dipole interaction, which is not strongly dependent on the position in the spectrum (Figure S5). In toluene:$CHCl_3$ solution at X-band the relaxation rates at 50 K for **1b**, **2a**, **2b** show little orientation dependence, similar to that observed for diradical **2a** in sucrose octaacetate.

Well-defined half-field transitions were observed for the diradicals.[2] At 15 to 80 K it was not possible to observe a spin echo, which is attributed to short values of T_m. Values of T_1 were measured by saturation recovery. Signal-to-noise is lower than for the allowed transitions so higher observe powers were used at half-field to observe the recovery, which introduces additional uncertainty in the values. Within that uncertainty, values of T_1 at half-field are similar to those for the allowed transitions. In CW experiments it has been observed that it is more difficult to saturate the half-field transitions than the allowed transitions.[3] The present results show that the difference in power saturation of the transitions is not due to differences in T_1, but must arise from shorter T_2 and/or the low transition probability for the forbidden transition.

The small dependence of $1/T_1$ on position in the spectrum for **3** is shown in figure S6. The orientation dependence is much less than for monoradicals. Since the nitroxyl rings are non-planar the z axes, which are long the p-π orbital of the nitroxyl nitrogen are not coincident. When the magnetic field is along the z axis for one half of the diradical, which would give a longer T_1 for the monoradical, the field is at an intermediate orientation for the other half of the diradical which would give a shorter T_1. Thus the exchange interaction averages the extremes of monoradical relaxation times.

(1) Du, J.-L.; Eaton, G. R.; Eaton, S. S. *J. Magn. Reson. A* 1995, *115*, 213.
(2) Rajca, A.; Mukherjee, S.; Pink, M.; Rajca, S. *J. Am. Chem. Soc.* 2006, *128*, 13497.
(3) Eaton, S. S.; Eaton, G. R. *J. Amer. Chem. Soc.* 1982, *104*, 5002.

DFT calculations on nitroxide diradical anti-4b at the UB3LYP/6-31G(d) level with Gaussian 03.
File: DiNO_C5dft.log

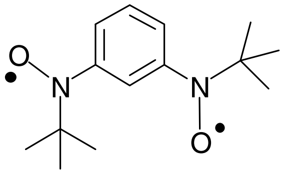

anti-**4b**

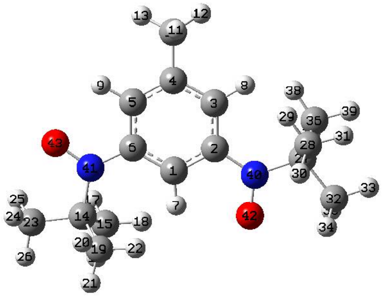

```
******************************************
 Gaussian 03:  IA32W-G03RevC.02 12-Jun-2004
               04-Oct-2007
 ******************************************
 %chk=DiNO_C5dft.chk
 %mem=8MW
 %nproc=1
 Will use up to    1 processors via shared memory.
 ----------------------------------------------
 # opt=tight freq ub3lyp/6-31g(d) geom=connectivity
 ----------------------------------------------

SCF Done:  E(UB+HF-LYP) =  -845.876631256     A.U. after    4 cycles
             Convg  =    0.6886D-08             -V/T =  2.0096
             S**2   =   2.0318
 Annihilation of the first spin contaminant:
 S**2 before annihilation     2.0318,   after     2.0005


Item               Value     Threshold  Converged?
 Maximum Force            0.000000     0.000015     YES
 RMS     Force            0.000000     0.000010     YES
 Maximum Displacement     0.000115     0.000060     NO
 RMS     Displacement     0.000021     0.000040     YES
 Predicted change in Energy=-5.713851D-12
 Optimization completed on the basis of negligible forces.
    -- Stationary point found.
                            ----------------------------
```

```
                           !   Optimized Parameters   !
                           ! (Angstroms and Degrees)  !
 --------------------------                            --------------------------
 ! Name  Definition              Value          Derivative Info.                !
 --------------------------------------------------------------------------------
 ! R1    R(1,2)                  1.4069         -DE/DX =    0.0                 !
 ! R2    R(1,6)                  1.3988         -DE/DX =    0.0                 !
 ! R3    R(1,7)                  1.0747         -DE/DX =    0.0                 !
 ! R4    R(2,3)                  1.406          -DE/DX =    0.0                 !
 ! R5    R(2,40)                 1.4211         -DE/DX =    0.0                 !
 ! R6    R(3,4)                  1.4017         -DE/DX =    0.0                 !
 ! R7    R(3,8)                  1.0799         -DE/DX =    0.0                 !
 ! R8    R(4,5)                  1.3909         -DE/DX =    0.0                 !
 ! R9    R(4,10)                 1.5127         -DE/DX =    0.0                 !
 ! R10   R(5,6)                  1.4119         -DE/DX =    0.0                 !
 ! R11   R(5,9)                  1.0817         -DE/DX =    0.0                 !
 ! R12   R(6,41)                 1.4179         -DE/DX =    0.0                 !
 ! R13   R(10,11)                1.098          -DE/DX =    0.0                 !
 ! R14   R(10,12)                1.0959         -DE/DX =    0.0                 !
 ! R15   R(10,13)                1.0941         -DE/DX =    0.0                 !
 ! R16   R(14,15)                1.5427         -DE/DX =    0.0                 !
 ! R17   R(14,19)                1.5428         -DE/DX =    0.0                 !
 ! R18   R(14,23)                1.537          -DE/DX =    0.0                 !
 ! R19   R(14,41)                1.519          -DE/DX =    0.0                 !
 ! R20   R(15,16)                1.0955         -DE/DX =    0.0                 !
 ! R21   R(15,17)                1.0952         -DE/DX =    0.0                 !
 ! R22   R(15,18)                1.0909         -DE/DX =    0.0                 !
 ! R23   R(19,20)                1.0952         -DE/DX =    0.0                 !
 ! R24   R(19,21)                1.0955         -DE/DX =    0.0                 !
 ! R25   R(19,22)                1.091          -DE/DX =    0.0                 !
 ! R26   R(23,24)                1.0919         -DE/DX =    0.0                 !
 ! R27   R(23,25)                1.092          -DE/DX =    0.0                 !
 ! R28   R(23,26)                1.0954         -DE/DX =    0.0                 !
 ! R29   R(27,28)                1.5424         -DE/DX =    0.0                 !
 ! R30   R(27,32)                1.5372         -DE/DX =    0.0                 !
 ! R31   R(27,36)                1.5425         -DE/DX =    0.0                 !
 ! R32   R(27,40)                1.5173         -DE/DX =    0.0                 !
 ! R33   R(28,29)                1.091          -DE/DX =    0.0                 !
 ! R34   R(28,30)                1.095          -DE/DX =    0.0                 !
 ! R35   R(28,31)                1.0955         -DE/DX =    0.0                 !
 ! R36   R(32,33)                1.0954         -DE/DX =    0.0                 !
 ! R37   R(32,34)                1.0919         -DE/DX =    0.0                 !
 ! R38   R(32,35)                1.0918         -DE/DX =    0.0                 !
 ! R39   R(36,37)                1.095          -DE/DX =    0.0                 !
 ! R40   R(36,38)                1.0911         -DE/DX =    0.0                 !
 ! R41   R(36,39)                1.0955         -DE/DX =    0.0                 !
 ! R42   R(40,42)                1.2841         -DE/DX =    0.0                 !
 ! R43   R(41,43)                1.2833         -DE/DX =    0.0                 !
 ! A1    A(2,1,6)              120.5084         -DE/DX =    0.0                 !
 ! A2    A(2,1,7)              116.4001         -DE/DX =    0.0                 !
 ! A3    A(6,1,7)              123.0913         -DE/DX =    0.0                 !
 ! A4    A(1,2,3)              119.4618         -DE/DX =    0.0                 !
 ! A5    A(1,2,40)             116.151          -DE/DX =    0.0                 !
 ! A6    A(3,2,40)             124.3867         -DE/DX =    0.0                 !
 ! A7    A(2,3,4)              120.1776         -DE/DX =    0.0                 !
 ! A8    A(2,3,8)              121.7118         -DE/DX =    0.0                 !
 ! A9    A(4,3,8)              118.1105         -DE/DX =    0.0                 !
 ! A10   A(3,4,5)              120.0488         -DE/DX =    0.0                 !
 ! A11   A(3,4,10)             119.6825         -DE/DX =    0.0                 !
 ! A12   A(5,4,10)             120.2604         -DE/DX =    0.0                 !
 ! A13   A(4,5,6)              120.466          -DE/DX =    0.0                 !
 ! A14   A(4,5,9)              121.0559         -DE/DX =    0.0                 !
 ! A15   A(6,5,9)              118.4781         -DE/DX =    0.0                 !
 ! A16   A(1,6,5)              119.3366         -DE/DX =    0.0                 !
 ! A17   A(1,6,41)             123.5723         -DE/DX =    0.0                 !
 ! A18   A(5,6,41)             117.091          -DE/DX =    0.0                 !
 ! A19   A(4,10,11)            111.1515         -DE/DX =    0.0                 !
```

```
! A20   A(4,10,12)            111.5226         -DE/DX =    0.0                 !
! A21   A(4,10,13)            111.2896         -DE/DX =    0.0                 !
! A22   A(11,10,12)           107.2114         -DE/DX =    0.0                 !
! A23   A(11,10,13)           107.4197         -DE/DX =    0.0                 !
! A24   A(12,10,13)           108.0446         -DE/DX =    0.0                 !
! A25   A(15,14,19)           112.7117         -DE/DX =    0.0                 !
! A26   A(15,14,23)           108.2595         -DE/DX =    0.0                 !
! A27   A(15,14,41)           110.1333         -DE/DX =    0.0                 !
! A28   A(19,14,23)           108.2718         -DE/DX =    0.0                 !
! A29   A(19,14,41)           110.0962         -DE/DX =    0.0                 !
! A30   A(23,14,41)           107.1794         -DE/DX =    0.0                 !
! A31   A(14,15,16)           109.0136         -DE/DX =    0.0                 !
! A32   A(14,15,17)           110.0739         -DE/DX =    0.0                 !
! A33   A(14,15,18)           113.8163         -DE/DX =    0.0                 !
! A34   A(16,15,17)           107.9942         -DE/DX =    0.0                 !
! A35   A(16,15,18)           107.6358         -DE/DX =    0.0                 !
! A36   A(17,15,18)           108.1283         -DE/DX =    0.0                 !
! A37   A(14,19,20)           110.0654         -DE/DX =    0.0                 !
! A38   A(14,19,21)           109.0358         -DE/DX =    0.0                 !
! A39   A(14,19,22)           113.7949         -DE/DX =    0.0                 !
! A40   A(20,19,21)           108.0014         -DE/DX =    0.0                 !
! A41   A(20,19,22)           108.1293         -DE/DX =    0.0                 !
! A42   A(21,19,22)           107.6368         -DE/DX =    0.0                 !
! A43   A(14,23,24)           111.5889         -DE/DX =    0.0                 !
! A44   A(14,23,25)           111.5714         -DE/DX =    0.0                 !
! A45   A(14,23,26)           108.151          -DE/DX =    0.0                 !
! A46   A(24,23,25)           107.9152         -DE/DX =    0.0                 !
! A47   A(24,23,26)           108.778          -DE/DX =    0.0                 !
! A48   A(25,23,26)           108.7685         -DE/DX =    0.0                 !
! A49   A(28,27,32)           108.138          -DE/DX =    0.0                 !
! A50   A(28,27,36)           112.8889         -DE/DX =    0.0                 !
! A51   A(28,27,40)           110.0898         -DE/DX =    0.0                 !
! A52   A(32,27,36)           108.1404         -DE/DX =    0.0                 !
! A53   A(32,27,40)           107.3676         -DE/DX =    0.0                 !
! A54   A(36,27,40)           110.0269         -DE/DX =    0.0                 !
! A55   A(27,28,29)           113.7676         -DE/DX =    0.0                 !
! A56   A(27,28,30)           110.0302         -DE/DX =    0.0                 !
! A57   A(27,28,31)           109.1743         -DE/DX =    0.0                 !
! A58   A(29,28,30)           107.9248         -DE/DX =    0.0                 !
! A59   A(29,28,31)           107.7548         -DE/DX =    0.0                 !
! A60   A(30,28,31)           108.0147         -DE/DX =    0.0                 !
! A61   A(27,32,33)           108.0989         -DE/DX =    0.0                 !
! A62   A(27,32,34)           111.5815         -DE/DX =    0.0                 !
! A63   A(27,32,35)           111.6002         -DE/DX =    0.0                 !
! A64   A(33,32,34)           108.784          -DE/DX =    0.0                 !
! A65   A(33,32,35)           108.7895         -DE/DX =    0.0                 !
! A66   A(34,32,35)           107.9198         -DE/DX =    0.0                 !
! A67   A(27,36,37)           110.0074         -DE/DX =    0.0                 !
! A68   A(27,36,38)           113.7542         -DE/DX =    0.0                 !
! A69   A(27,36,39)           109.2073         -DE/DX =    0.0                 !
! A70   A(37,36,38)           107.9161         -DE/DX =    0.0                 !
! A71   A(37,36,39)           108.0223         -DE/DX =    0.0                 !
! A72   A(38,36,39)           107.7601         -DE/DX =    0.0                 !
! A73   A(2,40,27)            125.9013         -DE/DX =    0.0                 !
! A74   A(2,40,42)            117.4558         -DE/DX =    0.0                 !
! A75   A(27,40,42)           116.6428         -DE/DX =    0.0                 !
! A76   A(6,41,14)            125.9136         -DE/DX =    0.0                 !
! A77   A(6,41,43)            117.2672         -DE/DX =    0.0                 !
! A78   A(14,41,43)           116.8192         -DE/DX =    0.0                 !
! D1    D(6,1,2,3)             -0.0012         -DE/DX =    0.0                 !
! D2    D(6,1,2,40)          -179.769          -DE/DX =    0.0                 !
! D3    D(7,1,2,3)            179.8294         -DE/DX =    0.0                 !
! D4    D(7,1,2,40)             0.0617         -DE/DX =    0.0                 !
! D5    D(2,1,6,5)             -0.0758         -DE/DX =    0.0                 !
! D6    D(2,1,6,41)           179.8304         -DE/DX =    0.0                 !
! D7    D(7,1,6,5)           -179.8948         -DE/DX =    0.0                 !
! D8    D(7,1,6,41)             0.0114         -DE/DX =    0.0                 !
```

```
! D9    D(1,2,3,4)              0.2229         -DE/DX =    0.0                 !
! D10   D(1,2,3,8)           -179.659          -DE/DX =    0.0                 !
! D11   D(40,2,3,4)           179.9702         -DE/DX =    0.0                 !
! D12   D(40,2,3,8)             0.0883         -DE/DX =    0.0                 !
! D13   D(1,2,40,27)         -179.2618         -DE/DX =    0.0                 !
! D14   D(1,2,40,42)            0.6091         -DE/DX =    0.0                 !
! D15   D(3,2,40,27)            0.9833         -DE/DX =    0.0                 !
! D16   D(3,2,40,42)         -179.1458         -DE/DX =    0.0                 !
! D17   D(2,3,4,5)             -0.3678         -DE/DX =    0.0                 !
! D18   D(2,3,4,10)           178.5862         -DE/DX =    0.0                 !
! D19   D(8,3,4,5)            179.5183         -DE/DX =    0.0                 !
! D20   D(8,3,4,10)            -1.5277         -DE/DX =    0.0                 !
! D21   D(3,4,5,6)              0.2904         -DE/DX =    0.0                 !
! D22   D(3,4,5,9)           -179.6559         -DE/DX =    0.0                 !
! D23   D(10,4,5,6)          -178.6575         -DE/DX =    0.0                 !
! D24   D(10,4,5,9)             1.3962         -DE/DX =    0.0                 !
! D25   D(3,4,10,11)          -80.3422         -DE/DX =    0.0                 !
! D26   D(3,4,10,12)           39.2375         -DE/DX =    0.0                 !
! D27   D(3,4,10,13)          159.9703         -DE/DX =    0.0                 !
! D28   D(5,4,10,11)           98.6095         -DE/DX =    0.0                 !
! D29   D(5,4,10,12)         -141.8108         -DE/DX =    0.0                 !
! D30   D(5,4,10,13)          -21.0779         -DE/DX =    0.0                 !
! D31   D(4,5,6,1)             -0.0689         -DE/DX =    0.0                 !
! D32   D(4,5,6,41)          -179.9811         -DE/DX =    0.0                 !
! D33   D(9,5,6,1)            179.8788         -DE/DX =    0.0                 !
! D34   D(9,5,6,41)            -0.0334         -DE/DX =    0.0                 !
! D35   D(1,6,41,14)           -0.6165         -DE/DX =    0.0                 !
! D36   D(1,6,41,43)          179.4199         -DE/DX =    0.0                 !
! D37   D(5,6,41,14)          179.2917         -DE/DX =    0.0                 !
! D38   D(5,6,41,43)           -0.6719         -DE/DX =    0.0                 !
! D39   D(19,14,15,16)         61.7935         -DE/DX =    0.0                 !
! D40   D(19,14,15,17)       -179.9247         -DE/DX =    0.0                 !
! D41   D(19,14,15,18)        -58.3639         -DE/DX =    0.0                 !
! D42   D(23,14,15,16)        -57.9418         -DE/DX =    0.0                 !
! D43   D(23,14,15,17)         60.34           -DE/DX =    0.0                 !
! D44   D(23,14,15,18)       -178.0992         -DE/DX =    0.0                 !
! D45   D(41,14,15,16)       -174.8282         -DE/DX =    0.0                 !
! D46   D(41,14,15,17)        -56.5464         -DE/DX =    0.0                 !
! D47   D(41,14,15,18)         65.0144         -DE/DX =    0.0                 !
! D48   D(15,14,19,20)        179.8856         -DE/DX =    0.0                 !
! D49   D(15,14,19,21)        -61.8156         -DE/DX =    0.0                 !
! D50   D(15,14,19,22)         58.3448         -DE/DX =    0.0                 !
! D51   D(23,14,19,20)        -60.3862         -DE/DX =    0.0                 !
! D52   D(23,14,19,21)         57.9126         -DE/DX =    0.0                 !
! D53   D(23,14,19,22)        178.073          -DE/DX =    0.0                 !
! D54   D(41,14,19,20)         56.4867         -DE/DX =    0.0                 !
! D55   D(41,14,19,21)        174.7855         -DE/DX =    0.0                 !
! D56   D(41,14,19,22)        -65.0541         -DE/DX =    0.0                 !
! D57   D(15,14,23,24)       -179.246          -DE/DX =    0.0                 !
! D58   D(15,14,23,25)        -58.4372         -DE/DX =    0.0                 !
! D59   D(15,14,23,26)         61.1473         -DE/DX =    0.0                 !
! D60   D(19,14,23,24)         58.2683         -DE/DX =    0.0                 !
! D61   D(19,14,23,25)        179.0772         -DE/DX =    0.0                 !
! D62   D(19,14,23,26)        -61.3384         -DE/DX =    0.0                 !
! D63   D(41,14,23,24)        -60.4702         -DE/DX =    0.0                 !
! D64   D(41,14,23,25)         60.3386         -DE/DX =    0.0                 !
! D65   D(41,14,23,26)        179.9231         -DE/DX =    0.0                 !
! D66   D(15,14,41,6)         -61.9619         -DE/DX =    0.0                 !
! D67   D(15,14,41,43)        118.0018         -DE/DX =    0.0                 !
! D68   D(19,14,41,6)          62.9288         -DE/DX =    0.0                 !
! D69   D(19,14,41,43)       -117.1074         -DE/DX =    0.0                 !
! D70   D(23,14,41,6)        -179.5192         -DE/DX =    0.0                 !
! D71   D(23,14,41,43)          0.4445         -DE/DX =    0.0                 !
! D72   D(32,27,28,29)        179.3379         -DE/DX =    0.0                 !
! D73   D(32,27,28,30)        -59.4311         -DE/DX =    0.0                 !
! D74   D(32,27,28,31)         58.9463         -DE/DX =    0.0                 !
! D75   D(36,27,28,29)         59.7387         -DE/DX =    0.0                 !
```

```
! D76   D(36,27,28,30)       -179.0304         -DE/DX =    0.0                 !
! D77   D(36,27,28,31)        -60.6529         -DE/DX =    0.0                 !
! D78   D(40,27,28,29)        -63.6439         -DE/DX =    0.0                 !
! D79   D(40,27,28,30)         57.587          -DE/DX =    0.0                 !
! D80   D(40,27,28,31)        175.9644         -DE/DX =    0.0                 !
! D81   D(28,27,32,33)        -61.176          -DE/DX =    0.0                 !
! D82   D(28,27,32,34)         58.4002         -DE/DX =    0.0                 !
! D83   D(28,27,32,35)        179.2298         -DE/DX =    0.0                 !
! D84   D(36,27,32,33)         61.3727         -DE/DX =    0.0                 !
! D85   D(36,27,32,34)       -179.0512         -DE/DX =    0.0                 !
! D86   D(36,27,32,35)        -58.2216         -DE/DX =    0.0                 !
! D87   D(40,27,32,33)       -179.9381         -DE/DX =    0.0                 !
! D88   D(40,27,32,34)        -60.3619         -DE/DX =    0.0                 !
! D89   D(40,27,32,35)         60.4676         -DE/DX =    0.0                 !
! D90   D(28,27,36,37)        179.0137         -DE/DX =    0.0                 !
! D91   D(28,27,36,38)        -59.7927         -DE/DX =    0.0                 !
! D92   D(28,27,36,39)         60.6205         -DE/DX =    0.0                 !
! D93   D(32,27,36,37)         59.4159         -DE/DX =    0.0                 !
! D94   D(32,27,36,38)       -179.3905         -DE/DX =    0.0                 !
! D95   D(32,27,36,39)        -58.9773         -DE/DX =    0.0                 !
! D96   D(40,27,36,37)        -57.5689         -DE/DX =    0.0                 !
! D97   D(40,27,36,38)         63.6248         -DE/DX =    0.0                 !
! D98   D(40,27,36,39)       -175.962          -DE/DX =    0.0                 !
! D99   D(28,27,40,2)          61.7512         -DE/DX =    0.0                 !
! D100  D(28,27,40,42)       -118.1207         -DE/DX =    0.0                 !
! D101  D(32,27,40,2)         179.248          -DE/DX =    0.0                 !
! D102  D(32,27,40,42)         -0.6239         -DE/DX =    0.0                 !
! D103  D(36,27,40,2)         -63.2863         -DE/DX =    0.0                 !
! D104  D(36,27,40,42)        116.8418         -DE/DX =    0.0                 !
--------------------------------------------------------------------------------
GradGradGradGradGradGradGradGradGradGradGradGradGradGradGradGradGradGrad

                         Input orientation:
---------------------------------------------------------------------
Center     Atomic     Atomic              Coordinates (Angstroms)
Number     Number      Type              X           Y           Z
---------------------------------------------------------------------
   1          6           0        0.128374    0.157637   -0.020905
   2          6           0        0.067122   -0.279707    1.314933
   3          6           0        1.259655   -0.539036    2.013031
   4          6           0        2.498554   -0.358180    1.382891
   5          6           0        2.551496    0.071561    0.061111
   6          6           0        1.362980    0.334720   -0.654258
   7          1           0       -0.812330    0.338349   -0.508166
   8          1           0        1.254900   -0.881186    3.037285
   9          1           0        3.498439    0.211189   -0.442766
  10          6           0        3.775143   -0.609653    2.154397
  11          1           0        4.027743    0.247387    2.792587
  12          1           0        3.684312   -1.484800    2.807704
  13          1           0        4.620504   -0.776353    1.480134
  14          6           0        0.362122    1.091956   -2.949712
  15          6           0       -0.501601   -0.163423   -3.190413
  16          1           0       -1.258811    0.064336   -3.948588
  17          1           0        0.120928   -0.981088   -3.568941
  18          1           0       -1.022061   -0.517510   -2.299435
  19          6           0       -0.456500    2.284154   -2.412468
  20          1           0        0.197296    3.148637   -2.255640
  21          1           0       -1.212685    2.561839   -3.154873
  22          1           0       -0.974405    2.075746   -1.475155
  23          6           0        0.994146    1.505568   -4.288319
  24          1           0        1.630707    2.385716   -4.177116
  25          1           0        1.601965    0.702585   -4.710428
  26          1           0        0.185808    1.741279   -4.988957
  27          6           0       -1.555839   -0.874503    3.280308
  28          6           0       -0.979435    0.135148    4.293921
  29          1           0        0.109373    0.201618    4.277617
  30          1           0       -1.381068    1.134688    4.097400
```

```
   31          1             0       -1.281097   -0.158355    5.305340
   32          6             0       -3.086326   -0.876119    3.424044
   33          1             0       -3.332040   -1.192466    4.443606
   34          1             0       -3.506832    0.116967    3.253075
   35          1             0       -3.555477   -1.565467    2.719266
   36          6             0       -1.050113   -2.313119    3.512753
   37          1             0       -1.500661   -2.991476    2.780755
   38          1             0        0.033878   -2.414758    3.441810
   39          1             0       -1.352080   -2.644196    4.512449
   40          7             0       -1.234354   -0.433077    1.864736
   41          7             0        1.500232    0.768764   -1.997069
   42          8             0       -2.233852   -0.174290    1.101268
   43          8             0        2.692390    0.901278   -2.453176
 ---------------------------------------------------------------------
```

DFT calculations on nitroxide diradical syn-4b at the UB3LYP/6-31G(d) level with Gaussian 03

File: DiNO_C4dft.log

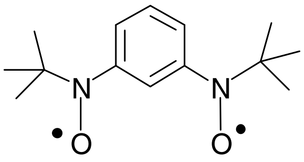

syn-**4b**

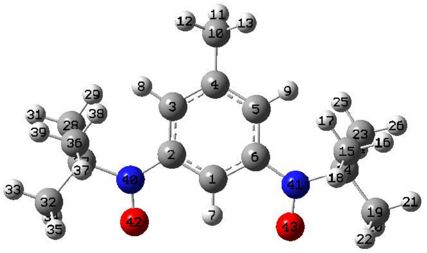

```
******************************************
 Gaussian 03:  IA32W-G03RevC.02 12-Jun-2004
                22-Oct-2007
 ******************************************
 %chk=DiNO_C4dft.chk
 %mem=8MW
 %nproc=1
 Will use up to    1 processors via shared memory.
 ----------------------------------------------
 # opt=tight freq ub3lyp/6-31g(d) geom=connectivity
 ----------------------------------------------

SCF Done:  E(UB+HF-LYP) =  -845.873725530     A.U. after   10 cycles
             Convg  =    0.7542D-08             -V/T =  2.0096
             S**2   =   2.0307
 Annihilation of the first spin contaminant:
 S**2 before annihilation     2.0307,   after     2.0005


Item               Value     Threshold  Converged?
 Maximum Force            0.000000     0.000015     YES
 RMS     Force            0.000000     0.000010     YES
 Maximum Displacement     0.013707     0.000060     NO
 RMS     Displacement     0.001876     0.000040     NO
 Predicted change in Energy=-1.466410D-09
 Optimization completed on the basis of negligible forces.
    -- Stationary point found.
                           ----------------------------
                           !   Optimized Parameters   !
                           ! (Angstroms and Degrees)  !
```

```
 --------------------------                            --------------------------
 ! Name  Definition              Value          Derivative Info.                !
 --------------------------------------------------------------------------------
 ! R1    R(1,2)                  1.402          -DE/DX =    0.0                 !
 ! R2    R(1,6)                  1.402          -DE/DX =    0.0                 !
 ! R3    R(1,7)                  1.078          -DE/DX =    0.0                 !
 ! R4    R(2,3)                  1.4096         -DE/DX =    0.0                 !
 ! R5    R(2,40)                 1.4206         -DE/DX =    0.0                 !
 ! R6    R(3,4)                  1.3967         -DE/DX =    0.0                 !
 ! R7    R(3,8)                  1.0798         -DE/DX =    0.0                 !
 ! R8    R(4,5)                  1.3966         -DE/DX =    0.0                 !
 ! R9    R(4,10)                 1.5132         -DE/DX =    0.0                 !
 ! R10   R(5,6)                  1.4097         -DE/DX =    0.0                 !
 ! R11   R(5,9)                  1.0798         -DE/DX =    0.0                 !
 ! R12   R(6,41)                 1.4206         -DE/DX =    0.0                 !
 ! R13   R(10,11)                1.0981         -DE/DX =    0.0                 !
 ! R14   R(10,12)                1.0951         -DE/DX =    0.0                 !
 ! R15   R(10,13)                1.0951         -DE/DX =    0.0                 !
 ! R16   R(14,15)                1.5423         -DE/DX =    0.0                 !
 ! R17   R(14,19)                1.5372         -DE/DX =    0.0                 !
 ! R18   R(14,23)                1.543          -DE/DX =    0.0                 !
 ! R19   R(14,41)                1.5176         -DE/DX =    0.0                 !
 ! R20   R(15,16)                1.0956         -DE/DX =    0.0                 !
 ! R21   R(15,17)                1.0909         -DE/DX =    0.0                 !
 ! R22   R(15,18)                1.095          -DE/DX =    0.0                 !
 ! R23   R(19,20)                1.0914         -DE/DX =    0.0                 !
 ! R24   R(19,21)                1.0955         -DE/DX =    0.0                 !
 ! R25   R(19,22)                1.0921         -DE/DX =    0.0                 !
 ! R26   R(23,24)                1.0949         -DE/DX =    0.0                 !
 ! R27   R(23,25)                1.0913         -DE/DX =    0.0                 !
 ! R28   R(23,26)                1.0956         -DE/DX =    0.0                 !
 ! R29   R(27,28)                1.543          -DE/DX =    0.0                 !
 ! R30   R(27,32)                1.5372         -DE/DX =    0.0                 !
 ! R31   R(27,36)                1.5422         -DE/DX =    0.0                 !
 ! R32   R(27,40)                1.5176         -DE/DX =    0.0                 !
 ! R33   R(28,29)                1.0913         -DE/DX =    0.0                 !
 ! R34   R(28,30)                1.0949         -DE/DX =    0.0                 !
 ! R35   R(28,31)                1.0956         -DE/DX =    0.0                 !
 ! R36   R(32,33)                1.0955         -DE/DX =    0.0                 !
 ! R37   R(32,34)                1.0914         -DE/DX =    0.0                 !
 ! R38   R(32,35)                1.0921         -DE/DX =    0.0                 !
 ! R39   R(36,37)                1.095          -DE/DX =    0.0                 !
 ! R40   R(36,38)                1.0909         -DE/DX =    0.0                 !
 ! R41   R(36,39)                1.0955         -DE/DX =    0.0                 !
 ! R42   R(40,42)                1.2823         -DE/DX =    0.0                 !
 ! R43   R(41,43)                1.2823         -DE/DX =    0.0                 !
 ! A1    A(2,1,6)              120.7063         -DE/DX =    0.0                 !
 ! A2    A(2,1,7)              119.6461         -DE/DX =    0.0                 !
 ! A3    A(6,1,7)              119.6464         -DE/DX =    0.0                 !
 ! A4    A(1,2,3)              119.3258         -DE/DX =    0.0                 !
 ! A5    A(1,2,40)             116.681          -DE/DX =    0.0                 !
 ! A6    A(3,2,40)             123.9926         -DE/DX =    0.0                 !
 ! A7    A(2,3,4)              120.2365         -DE/DX =    0.0                 !
 ! A8    A(2,3,8)              121.6546         -DE/DX =    0.0                 !
 ! A9    A(4,3,8)              118.1052         -DE/DX =    0.0                 !
 ! A10   A(3,4,5)              120.1657         -DE/DX =    0.0                 !
 ! A11   A(3,4,10)             119.9055         -DE/DX =    0.0                 !
 ! A12   A(5,4,10)             119.9076         -DE/DX =    0.0                 !
 ! A13   A(4,5,6)              120.2384         -DE/DX =    0.0                 !
 ! A14   A(4,5,9)              118.1012         -DE/DX =    0.0                 !
 ! A15   A(6,5,9)              121.6568         -DE/DX =    0.0                 !
 ! A16   A(1,6,5)              119.3228         -DE/DX =    0.0                 !
 ! A17   A(1,6,41)             116.6804         -DE/DX =    0.0                 !
 ! A18   A(5,6,41)             123.9964         -DE/DX =    0.0                 !
 ! A19   A(4,10,11)            111.221          -DE/DX =    0.0                 !
 ! A20   A(4,10,12)            111.4995         -DE/DX =    0.0                 !
 ! A21   A(4,10,13)            111.4995         -DE/DX =    0.0                 !
```

```
 ! A22   A(11,10,12)           107.2662         -DE/DX =    0.0                 !
 ! A23   A(11,10,13)           107.2677         -DE/DX =    0.0                 !
 ! A24   A(12,10,13)           107.8684         -DE/DX =    0.0                 !
 ! A25   A(15,14,19)           108.0895         -DE/DX =    0.0                 !
 ! A26   A(15,14,23)           112.8586         -DE/DX =    0.0                 !
 ! A27   A(15,14,41)           110.2137         -DE/DX =    0.0                 !
 ! A28   A(19,14,23)           108.205          -DE/DX =    0.0                 !
 ! A29   A(19,14,41)           107.2873         -DE/DX =    0.0                 !
 ! A30   A(23,14,41)           109.9928         -DE/DX =    0.0                 !
 ! A31   A(14,15,16)           109.1436         -DE/DX =    0.0                 !
 ! A32   A(14,15,17)           113.8279         -DE/DX =    0.0                 !
 ! A33   A(14,15,18)           110.0402         -DE/DX =    0.0                 !
 ! A34   A(16,15,17)           107.7503         -DE/DX =    0.0                 !
 ! A35   A(16,15,18)           107.9933         -DE/DX =    0.0                 !
 ! A36   A(17,15,18)           107.9073         -DE/DX =    0.0                 !
 ! A37   A(14,19,20)           111.6082         -DE/DX =    0.0                 !
 ! A38   A(14,19,21)           108.18           -DE/DX =    0.0                 !
 ! A39   A(14,19,22)           111.4333         -DE/DX =    0.0                 !
 ! A40   A(20,19,21)           108.856          -DE/DX =    0.0                 !
 ! A41   A(20,19,22)           107.9141         -DE/DX =    0.0                 !
 ! A42   A(21,19,22)           108.7864         -DE/DX =    0.0                 !
 ! A43   A(14,23,24)           109.9649         -DE/DX =    0.0                 !
 ! A44   A(14,23,25)           113.6868         -DE/DX =    0.0                 !
 ! A45   A(14,23,26)           109.2733         -DE/DX =    0.0                 !
 ! A46   A(24,23,25)           107.943          -DE/DX =    0.0                 !
 ! A47   A(24,23,26)           108.0692         -DE/DX =    0.0                 !
 ! A48   A(25,23,26)           107.7357         -DE/DX =    0.0                 !
 ! A49   A(28,27,32)           108.2076         -DE/DX =    0.0                 !
 ! A50   A(28,27,36)           112.8567         -DE/DX =    0.0                 !
 ! A51   A(28,27,40)           109.9893         -DE/DX =    0.0                 !
 ! A52   A(32,27,36)           108.0894         -DE/DX =    0.0                 !
 ! A53   A(32,27,40)           107.2861         -DE/DX =    0.0                 !
 ! A54   A(36,27,40)           110.2178         -DE/DX =    0.0                 !
 ! A55   A(27,28,29)           113.6835         -DE/DX =    0.0                 !
 ! A56   A(27,28,30)           109.964          -DE/DX =    0.0                 !
 ! A57   A(27,28,31)           109.2757         -DE/DX =    0.0                 !
 ! A58   A(29,28,30)           107.9443         -DE/DX =    0.0                 !
 ! A59   A(29,28,31)           107.7352         -DE/DX =    0.0                 !
 ! A60   A(30,28,31)           108.0705         -DE/DX =    0.0                 !
 ! A61   A(27,32,33)           108.1812         -DE/DX =    0.0                 !
 ! A62   A(27,32,34)           111.6102         -DE/DX =    0.0                 !
 ! A63   A(27,32,35)           111.4315         -DE/DX =    0.0                 !
 ! A64   A(33,32,34)           108.8563         -DE/DX =    0.0                 !
 ! A65   A(33,32,35)           108.7846         -DE/DX =    0.0                 !
 ! A66   A(34,32,35)           107.9142         -DE/DX =    0.0                 !
 ! A67   A(27,36,37)           110.042          -DE/DX =    0.0                 !
 ! A68   A(27,36,38)           113.8286         -DE/DX =    0.0                 !
 ! A69   A(27,36,39)           109.1412         -DE/DX =    0.0                 !
 ! A70   A(37,36,38)           107.9076         -DE/DX =    0.0                 !
 ! A71   A(37,36,39)           107.9926         -DE/DX =    0.0                 !
 ! A72   A(38,36,39)           107.7503         -DE/DX =    0.0                 !
 ! A73   A(2,40,27)            125.898          -DE/DX =    0.0                 !
 ! A74   A(2,40,42)            117.4357         -DE/DX =    0.0                 !
 ! A75   A(27,40,42)           116.6608         -DE/DX =    0.0                 !
 ! A76   A(6,41,14)            125.8993         -DE/DX =    0.0                 !
 ! A77   A(6,41,43)            117.4364         -DE/DX =    0.0                 !
 ! A78   A(14,41,43)           116.6591         -DE/DX =    0.0                 !
 ! D1    D(6,1,2,3)              0.5235         -DE/DX =    0.0                 !
 ! D2    D(6,1,2,40)          -179.7436         -DE/DX =    0.0                 !
 ! D3    D(7,1,2,3)           -179.8764         -DE/DX =    0.0                 !
 ! D4    D(7,1,2,40)            -0.1435         -DE/DX =    0.0                 !
 ! D5    D(2,1,6,5)             -0.5207         -DE/DX =    0.0                 !
 ! D6    D(2,1,6,41)           179.7272         -DE/DX =    0.0                 !
 ! D7    D(7,1,6,5)            179.8792         -DE/DX =    0.0                 !
 ! D8    D(7,1,6,41)             0.1271         -DE/DX =    0.0                 !
 ! D9    D(1,2,3,4)              0.0271         -DE/DX =    0.0                 !
 ! D10   D(1,2,3,8)            179.3077         -DE/DX =    0.0                 !
```

```
! D11   D(40,2,3,4)          -179.6851         -DE/DX =    0.0                 !
! D12   D(40,2,3,8)            -0.4045         -DE/DX =    0.0                 !
! D13   D(1,2,40,27)          173.2829         -DE/DX =    0.0                 !
! D14   D(1,2,40,42)           -5.8328         -DE/DX =    0.0                 !
! D15   D(3,2,40,27)           -6.9979         -DE/DX =    0.0                 !
! D16   D(3,2,40,42)          173.8864         -DE/DX =    0.0                 !
! D17   D(2,3,4,5)             -0.5763         -DE/DX =    0.0                 !
! D18   D(2,3,4,10)           177.7459         -DE/DX =    0.0                 !
! D19   D(8,3,4,5)           -179.8821         -DE/DX =    0.0                 !
! D20   D(8,3,4,10)            -1.5599         -DE/DX =    0.0                 !
! D21   D(3,4,5,6)              0.5791         -DE/DX =    0.0                 !
! D22   D(3,4,5,9)            179.9            -DE/DX =    0.0                 !
! D23   D(10,4,5,6)          -177.743          -DE/DX =    0.0                 !
! D24   D(10,4,5,9)             1.5779         -DE/DX =    0.0                 !
! D25   D(3,4,10,11)          -89.0926         -DE/DX =    0.0                 !
! D26   D(3,4,10,12)           30.588          -DE/DX =    0.0                 !
! D27   D(3,4,10,13)          151.225          -DE/DX =    0.0                 !
! D28   D(5,4,10,11)           89.2339         -DE/DX =    0.0                 !
! D29   D(5,4,10,12)         -151.0855         -DE/DX =    0.0                 !
! D30   D(5,4,10,13)          -30.4485         -DE/DX =    0.0                 !
! D31   D(4,5,6,1)             -0.0327         -DE/DX =    0.0                 !
! D32   D(4,5,6,41)           179.7002         -DE/DX =    0.0                 !
! D33   D(9,5,6,1)           -179.3289         -DE/DX =    0.0                 !
! D34   D(9,5,6,41)             0.4039         -DE/DX =    0.0                 !
! D35   D(1,6,41,14)         -173.4745         -DE/DX =    0.0                 !
! D36   D(1,6,41,43)            5.6641         -DE/DX =    0.0                 !
! D37   D(5,6,41,14)            6.7862         -DE/DX =    0.0                 !
! D38   D(5,6,41,43)         -174.0752         -DE/DX =    0.0                 !
! D39   D(19,14,15,16)         59.4514         -DE/DX =    0.0                 !
! D40   D(19,14,15,17)        179.8552         -DE/DX =    0.0                 !
! D41   D(19,14,15,18)        -58.8873         -DE/DX =    0.0                 !
! D42   D(23,14,15,16)        -60.1772         -DE/DX =    0.0                 !
! D43   D(23,14,15,17)         60.2266         -DE/DX =    0.0                 !
! D44   D(23,14,15,18)       -178.5159         -DE/DX =    0.0                 !
! D45   D(41,14,15,16)        176.4136         -DE/DX =    0.0                 !
! D46   D(41,14,15,17)        -63.1825         -DE/DX =    0.0                 !
! D47   D(41,14,15,18)         58.0749         -DE/DX =    0.0                 !
! D48   D(15,14,19,20)        179.9495         -DE/DX =    0.0                 !
! D49   D(15,14,19,21)        -60.3174         -DE/DX =    0.0                 !
! D50   D(15,14,19,22)         59.2248         -DE/DX =    0.0                 !
! D51   D(23,14,19,20)        -57.5289         -DE/DX =    0.0                 !
! D52   D(23,14,19,21)         62.2042         -DE/DX =    0.0                 !
! D53   D(23,14,19,22)       -178.2537         -DE/DX =    0.0                 !
! D54   D(41,14,19,20)         61.1108         -DE/DX =    0.0                 !
! D55   D(41,14,19,21)       -179.156          -DE/DX =    0.0                 !
! D56   D(41,14,19,22)        -59.6139         -DE/DX =    0.0                 !
! D57   D(15,14,23,24)        179.7525         -DE/DX =    0.0                 !
! D58   D(15,14,23,25)        -59.0968         -DE/DX =    0.0                 !
! D59   D(15,14,23,26)         61.2877         -DE/DX =    0.0                 !
! D60   D(19,14,23,24)         60.1906         -DE/DX =    0.0                 !
! D61   D(19,14,23,25)       -178.6588         -DE/DX =    0.0                 !
! D62   D(19,14,23,26)        -58.2742         -DE/DX =    0.0                 !
! D63   D(41,14,23,24)        -56.7161         -DE/DX =    0.0                 !
! D64   D(41,14,23,25)         64.4346         -DE/DX =    0.0                 !
! D65   D(41,14,23,26)       -175.1809         -DE/DX =    0.0                 !
! D66   D(15,14,41,6)          57.5048         -DE/DX =    0.0                 !
! D67   D(15,14,41,43)       -121.6398         -DE/DX =    0.0                 !
! D68   D(19,14,41,6)         174.9646         -DE/DX =    0.0                 !
! D69   D(19,14,41,43)         -4.18           -DE/DX =    0.0                 !
! D70   D(23,14,41,6)         -67.5571         -DE/DX =    0.0                 !
! D71   D(23,14,41,43)        113.2984         -DE/DX =    0.0                 !
! D72   D(32,27,28,29)        178.6336         -DE/DX =    0.0                 !
! D73   D(32,27,28,30)        -60.2171         -DE/DX =    0.0                 !
! D74   D(32,27,28,31)         58.2502         -DE/DX =    0.0                 !
! D75   D(36,27,28,29)         59.0711         -DE/DX =    0.0                 !
! D76   D(36,27,28,30)       -179.7796         -DE/DX =    0.0                 !
! D77   D(36,27,28,31)        -61.3123         -DE/DX =    0.0                 !
```

```
 ! D78   D(40,27,28,29)        -64.4617         -DE/DX =    0.0                 !
 ! D79   D(40,27,28,30)         56.6876         -DE/DX =    0.0                 !
 ! D80   D(40,27,28,31)        175.1549         -DE/DX =    0.0                 !
 ! D81   D(28,27,32,33)        -62.227          -DE/DX =    0.0                 !
 ! D82   D(28,27,32,34)         57.5085         -DE/DX =    0.0                 !
 ! D83   D(28,27,32,35)        178.2335         -DE/DX =    0.0                 !
 ! D84   D(36,27,32,33)         60.2939         -DE/DX =    0.0                 !
 ! D85   D(36,27,32,34)       -179.9706         -DE/DX =    0.0                 !
 ! D86   D(36,27,32,35)        -59.2457         -DE/DX =    0.0                 !
 ! D87   D(40,27,32,33)        179.1367         -DE/DX =    0.0                 !
 ! D88   D(40,27,32,34)        -61.1278         -DE/DX =    0.0                 !
 ! D89   D(40,27,32,35)         59.5972         -DE/DX =    0.0                 !
 ! D90   D(28,27,36,37)        178.5234         -DE/DX =    0.0                 !
 ! D91   D(28,27,36,38)        -60.2168         -DE/DX =    0.0                 !
 ! D92   D(28,27,36,39)         60.1858         -DE/DX =    0.0                 !
 ! D93   D(32,27,36,37)         58.8928         -DE/DX =    0.0                 !
 ! D94   D(32,27,36,38)       -179.8475         -DE/DX =    0.0                 !
 ! D95   D(32,27,36,39)        -59.4449         -DE/DX =    0.0                 !
 ! D96   D(40,27,36,37)        -58.0703         -DE/DX =    0.0                 !
 ! D97   D(40,27,36,38)         63.1895         -DE/DX =    0.0                 !
 ! D98   D(40,27,36,39)       -176.4079         -DE/DX =    0.0                 !
 ! D99   D(28,27,40,2)          67.7111         -DE/DX =    0.0                 !
 ! D100  D(28,27,40,42)       -113.1671         -DE/DX =    0.0                 !
 ! D101  D(32,27,40,2)        -174.8101         -DE/DX =    0.0                 !
 ! D102  D(32,27,40,42)          4.3117         -DE/DX =    0.0                 !
 ! D103  D(36,27,40,2)         -57.3488         -DE/DX =    0.0                 !
 ! D104  D(36,27,40,42)        121.7729         -DE/DX =    0.0                 !
 --------------------------------------------------------------------------------
 GradGradGradGradGradGradGradGradGradGradGradGradGradGradGradGradGradGrad

                          Input orientation:
 ---------------------------------------------------------------------
 Center     Atomic     Atomic              Coordinates (Angstroms)
 Number     Number      Type              X           Y           Z
 ---------------------------------------------------------------------
    1          6           0       -0.087431   -0.663471   -0.029287
    2          6           0       -0.092106   -0.626378    1.372197
    3          6           0        1.134579   -0.607916    2.066454
    4          6           0        2.341100   -0.625874    1.363155
    5          6           0        2.339160   -0.674392   -0.032645
    6          6           0        1.120324   -0.693229   -0.740633
    7          1           0       -1.022556   -0.675708   -0.565508
    8          1           0        1.174889   -0.568263    3.144768
    9          1           0        3.290928   -0.685333   -0.542507
   10          6           0        3.653072   -0.554306    2.113801
   11          1           0        3.969020    0.486621    2.263609
   12          1           0        3.574750   -1.015912    3.103809
   13          1           0        4.455598   -1.062369    1.568694
   14          6           0        2.183418   -0.912813   -3.122094
   15          6           0        2.937333   -2.222733   -2.815034
   16          1           0        3.728198   -2.365104   -3.559678
   17          1           0        3.402078   -2.242829   -1.828297
   18          1           0        2.252363   -3.074467   -2.882008
   19          6           0        1.588129   -1.024652   -4.534911
   20          1           0        1.038263   -0.123457   -4.811870
   21          1           0        2.411982   -1.168247   -5.242561
   22          1           0        0.904702   -1.872778   -4.614008
   23          6           0        3.098347    0.329016   -3.081404
   24          1           0        2.517707    1.228824   -3.309673
   25          1           0        3.588944    0.480766   -2.118462
   26          1           0        3.880343    0.227148   -3.842014
   27          6           0       -1.616072   -0.706985    3.498378
   28          6           0       -1.086307    0.554699    4.211397
   29          1           0       -0.003711    0.674611    4.143515
   30          1           0       -1.552187    1.448849    3.784369
   31          1           0       -1.350967    0.507898    5.273558
   32          6           0       -3.138582   -0.769550    3.700872
```

```
   33          1             0       -3.337201   -0.860037    4.774411
   34          1             0       -3.631268    0.129089    3.325504
   35          1             0       -3.574198   -1.630230    3.188870
   36          6             0       -1.005228   -2.009781    4.053442
   37          1             0       -1.431143   -2.874860    3.534444
   38          1             0        0.080255   -2.062857    3.958842
   39          1             0       -1.252496   -2.097798    5.117087
   40          7             0       -1.363572   -0.603788    2.005478
   41          7             0        1.025267   -0.735869   -2.157435
   42          8             0       -2.396846   -0.503252    1.252750
   43          8             0       -0.143490   -0.631510   -2.674603
 ---------------------------------------------------------------------
```

DFT calculations on nitroxide diradical 4a at the UB3LYP/6-31G(d) level with Gaussian 03

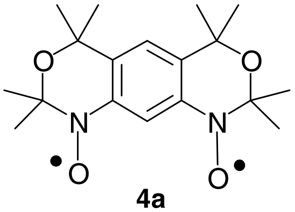

4a

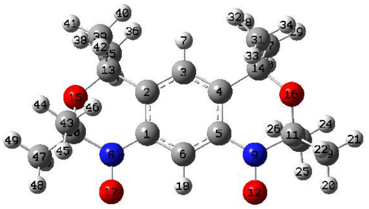

```
*******************************************
 Gaussian 03:  IA32W-G03RevC.02 12-Jun-2004
                28-Sep-2007
 *******************************************
 %chk=C:\G03W\Radicals\Oxazene NO\Freq_Oxaxene_MTDiNO_B3LYP_S1r1.chk
 %mem=6MW
 %nproc=1
 Will use up to    1 processors via shared memory.
 --------------------------------------------
 # opt freq ub3lyp/6-31g(d) geom=connectivity
 --------------------------------------------

SCF Done:  E(UB+HF-LYP) =  -1111.85524353     A.U. after   18 cycles
             Convg  =    0.9640D-08             -V/T =  2.0093
             S**2   =   2.0340
 Annihilation of the first spin contaminant:
 S**2 before annihilation     2.0340,   after     2.0006


Item               Value     Threshold  Converged?
 Maximum Force            0.000006     0.000450     YES
 RMS     Force            0.000002     0.000300     YES
 Maximum Displacement     0.000554     0.001800     YES
 RMS     Displacement     0.000103     0.001200     YES
 Predicted change in Energy=-4.120980D-09
 Optimization completed.
    -- Stationary point found.
                           ----------------------------
                           !   Optimized Parameters   !
                           ! (Angstroms and Degrees)  !
 --------------------------                            --------------------------
 ! Name  Definition              Value          Derivative Info.                !
 --------------------------------------------------------------------------------
 ! R1    R(1,2)                  1.4141         -DE/DX =    0.0                 !
```

```
 ! R2    R(1,6)                  1.3979         -DE/DX =    0.0                 !
 ! R3    R(1,8)                  1.3998         -DE/DX =    0.0                 !
 ! R4    R(2,3)                  1.3968         -DE/DX =    0.0                 !
 ! R5    R(2,13)                 1.522          -DE/DX =    0.0                 !
 ! R6    R(3,4)                  1.3968         -DE/DX =    0.0                 !
 ! R7    R(3,7)                  1.0862         -DE/DX =    0.0                 !
 ! R8    R(4,5)                  1.4141         -DE/DX =    0.0                 !
 ! R9    R(4,14)                 1.522          -DE/DX =    0.0                 !
 ! R10   R(5,6)                  1.3979         -DE/DX =    0.0                 !
 ! R11   R(5,9)                  1.3998         -DE/DX =    0.0                 !
 ! R12   R(6,18)                 1.0806         -DE/DX =    0.0                 !
 ! R13   R(8,10)                 1.4964         -DE/DX =    0.0                 !
 ! R14   R(8,17)                 1.279          -DE/DX =    0.0                 !
 ! R15   R(9,11)                 1.4964         -DE/DX =    0.0                 !
 ! R16   R(9,12)                 1.279          -DE/DX =    0.0                 !
 ! R17   R(10,15)                1.4146         -DE/DX =    0.0                 !
 ! R18   R(10,43)                1.5373         -DE/DX =    0.0                 !
 ! R19   R(10,47)                1.5264         -DE/DX =    0.0                 !
 ! R20   R(11,16)                1.4146         -DE/DX =    0.0                 !
 ! R21   R(11,19)                1.5264         -DE/DX =    0.0                 !
 ! R22   R(11,23)                1.5373         -DE/DX =    0.0                 !
 ! R23   R(13,15)                1.4453         -DE/DX =    0.0                 !
 ! R24   R(13,35)                1.5401         -DE/DX =    0.0                 !
 ! R25   R(13,39)                1.5415         -DE/DX =    0.0                 !
 ! R26   R(14,16)                1.4453         -DE/DX =    0.0                 !
 ! R27   R(14,27)                1.5415         -DE/DX =    0.0                 !
 ! R28   R(14,31)                1.5401         -DE/DX =    0.0                 !
 ! R29   R(19,20)                1.0902         -DE/DX =    0.0                 !
 ! R30   R(19,21)                1.0936         -DE/DX =    0.0                 !
 ! R31   R(19,22)                1.0929         -DE/DX =    0.0                 !
 ! R32   R(23,24)                1.0941         -DE/DX =    0.0                 !
 ! R33   R(23,25)                1.094          -DE/DX =    0.0                 !
 ! R34   R(23,26)                1.0931         -DE/DX =    0.0                 !
 ! R35   R(27,28)                1.0953         -DE/DX =    0.0                 !
 ! R36   R(27,29)                1.0948         -DE/DX =    0.0                 !
 ! R37   R(27,30)                1.0922         -DE/DX =    0.0                 !
 ! R38   R(31,32)                1.0943         -DE/DX =    0.0                 !
 ! R39   R(31,33)                1.0934         -DE/DX =    0.0                 !
 ! R40   R(31,34)                1.0949         -DE/DX =    0.0                 !
 ! R41   R(35,36)                1.0943         -DE/DX =    0.0                 !
 ! R42   R(35,37)                1.0934         -DE/DX =    0.0                 !
 ! R43   R(35,38)                1.0949         -DE/DX =    0.0                 !
 ! R44   R(39,40)                1.0953         -DE/DX =    0.0                 !
 ! R45   R(39,41)                1.0948         -DE/DX =    0.0                 !
 ! R46   R(39,42)                1.0922         -DE/DX =    0.0                 !
 ! R47   R(43,44)                1.0941         -DE/DX =    0.0                 !
 ! R48   R(43,45)                1.0939         -DE/DX =    0.0                 !
 ! R49   R(43,46)                1.0931         -DE/DX =    0.0                 !
 ! R50   R(47,48)                1.0902         -DE/DX =    0.0                 !
 ! R51   R(47,49)                1.0936         -DE/DX =    0.0                 !
 ! R52   R(47,50)                1.0929         -DE/DX =    0.0                 !
 ! A1    A(2,1,6)              121.0099         -DE/DX =    0.0                 !
 ! A2    A(2,1,8)              119.972          -DE/DX =    0.0                 !
 ! A3    A(6,1,8)              119.0139         -DE/DX =    0.0                 !
 ! A4    A(1,2,3)              117.5756         -DE/DX =    0.0                 !
 ! A5    A(1,2,13)             121.1151         -DE/DX =    0.0                 !
 ! A6    A(3,2,13)             121.2589         -DE/DX =    0.0                 !
 ! A7    A(2,3,4)              123.1597         -DE/DX =    0.0                 !
 ! A8    A(2,3,7)              118.4202         -DE/DX =    0.0                 !
 ! A9    A(4,3,7)              118.4201         -DE/DX =    0.0                 !
 ! A10   A(3,4,5)              117.5756         -DE/DX =    0.0                 !
 ! A11   A(3,4,14)             121.2588         -DE/DX =    0.0                 !
 ! A12   A(5,4,14)             121.1152         -DE/DX =    0.0                 !
 ! A13   A(4,5,6)              121.0098         -DE/DX =    0.0                 !
 ! A14   A(4,5,9)              119.9722         -DE/DX =    0.0                 !
 ! A15   A(6,5,9)              119.0137         -DE/DX =    0.0                 !
 ! A16   A(1,6,5)              119.5876         -DE/DX =    0.0                 !
```

```
! A17   A(1,6,18)             120.2062         -DE/DX =    0.0                 !
! A18   A(5,6,18)             120.2062         -DE/DX =    0.0                 !
! A19   A(1,8,10)             119.1342         -DE/DX =    0.0                 !
! A20   A(1,8,17)             121.1201         -DE/DX =    0.0                 !
! A21   A(10,8,17)            118.2972         -DE/DX =    0.0                 !
! A22   A(5,9,11)             119.1343         -DE/DX =    0.0                 !
! A23   A(5,9,12)             121.1201         -DE/DX =    0.0                 !
! A24   A(11,9,12)            118.2972         -DE/DX =    0.0                 !
! A25   A(8,10,15)            109.1165         -DE/DX =    0.0                 !
! A26   A(8,10,43)            107.8879         -DE/DX =    0.0                 !
! A27   A(8,10,47)            108.9441         -DE/DX =    0.0                 !
! A28   A(15,10,43)           114.1742         -DE/DX =    0.0                 !
! A29   A(15,10,47)           105.117          -DE/DX =    0.0                 !
! A30   A(43,10,47)           111.4908         -DE/DX =    0.0                 !
! A31   A(9,11,16)            109.1165         -DE/DX =    0.0                 !
! A32   A(9,11,19)            108.9437         -DE/DX =    0.0                 !
! A33   A(9,11,23)            107.8876         -DE/DX =    0.0                 !
! A34   A(16,11,19)           105.1164         -DE/DX =    0.0                 !
! A35   A(16,11,23)           114.1759         -DE/DX =    0.0                 !
! A36   A(19,11,23)           111.4901         -DE/DX =    0.0                 !
! A37   A(2,13,15)            111.0969         -DE/DX =    0.0                 !
! A38   A(2,13,35)            110.1798         -DE/DX =    0.0                 !
! A39   A(2,13,39)            112.6354         -DE/DX =    0.0                 !
! A40   A(15,13,35)           102.8563         -DE/DX =    0.0                 !
! A41   A(15,13,39)           110.0406         -DE/DX =    0.0                 !
! A42   A(35,13,39)           109.5908         -DE/DX =    0.0                 !
! A43   A(4,14,16)            111.0968         -DE/DX =    0.0                 !
! A44   A(4,14,27)            112.6359         -DE/DX =    0.0                 !
! A45   A(4,14,31)            110.1793         -DE/DX =    0.0                 !
! A46   A(16,14,27)           110.042          -DE/DX =    0.0                 !
! A47   A(16,14,31)           102.8556         -DE/DX =    0.0                 !
! A48   A(27,14,31)           109.5899         -DE/DX =    0.0                 !
! A49   A(10,15,13)           122.118          -DE/DX =    0.0                 !
! A50   A(11,16,14)           122.1193         -DE/DX =    0.0                 !
! A51   A(11,19,20)           110.6554         -DE/DX =    0.0                 !
! A52   A(11,19,21)           108.7195         -DE/DX =    0.0                 !
! A53   A(11,19,22)           109.7515         -DE/DX =    0.0                 !
! A54   A(20,19,21)           109.7477         -DE/DX =    0.0                 !
! A55   A(20,19,22)           109.1404         -DE/DX =    0.0                 !
! A56   A(21,19,22)           108.7988         -DE/DX =    0.0                 !
! A57   A(11,23,24)           109.7843         -DE/DX =    0.0                 !
! A58   A(11,23,25)           109.2112         -DE/DX =    0.0                 !
! A59   A(11,23,26)           111.7446         -DE/DX =    0.0                 !
! A60   A(24,23,25)           109.1508         -DE/DX =    0.0                 !
! A61   A(24,23,26)           108.9729         -DE/DX =    0.0                 !
! A62   A(25,23,26)           107.9255         -DE/DX =    0.0                 !
! A63   A(14,27,28)           110.7529         -DE/DX =    0.0                 !
! A64   A(14,27,29)           109.2049         -DE/DX =    0.0                 !
! A65   A(14,27,30)           112.1626         -DE/DX =    0.0                 !
! A66   A(28,27,29)           108.2375         -DE/DX =    0.0                 !
! A67   A(28,27,30)           107.7919         -DE/DX =    0.0                 !
! A68   A(29,27,30)           108.5873         -DE/DX =    0.0                 !
! A69   A(14,31,32)           111.1818         -DE/DX =    0.0                 !
! A70   A(14,31,33)           110.1439         -DE/DX =    0.0                 !
! A71   A(14,31,34)           109.4655         -DE/DX =    0.0                 !
! A72   A(32,31,33)           108.769          -DE/DX =    0.0                 !
! A73   A(32,31,34)           108.6414         -DE/DX =    0.0                 !
! A74   A(33,31,34)           108.5842         -DE/DX =    0.0                 !
! A75   A(13,35,36)           111.1818         -DE/DX =    0.0                 !
! A76   A(13,35,37)           110.144          -DE/DX =    0.0                 !
! A77   A(13,35,38)           109.4655         -DE/DX =    0.0                 !
! A78   A(36,35,37)           108.7689         -DE/DX =    0.0                 !
! A79   A(36,35,38)           108.6414         -DE/DX =    0.0                 !
! A80   A(37,35,38)           108.5842         -DE/DX =    0.0                 !
! A81   A(13,39,40)           110.7529         -DE/DX =    0.0                 !
! A82   A(13,39,41)           109.205          -DE/DX =    0.0                 !
! A83   A(13,39,42)           112.1621         -DE/DX =    0.0                 !
```

```
! A84   A(40,39,41)          108.2376         -DE/DX =    0.0                 !
! A85   A(40,39,42)          107.7921         -DE/DX =    0.0                 !
! A86   A(41,39,42)          108.5873         -DE/DX =    0.0                 !
! A87   A(10,43,44)          109.7842         -DE/DX =    0.0                 !
! A88   A(10,43,45)          109.2114         -DE/DX =    0.0                 !
! A89   A(10,43,46)          111.7444         -DE/DX =    0.0                 !
! A90   A(44,43,45)          109.1509         -DE/DX =    0.0                 !
! A91   A(44,43,46)          108.9727         -DE/DX =    0.0                 !
! A92   A(45,43,46)          107.9257         -DE/DX =    0.0                 !
! A93   A(10,47,48)          110.6554         -DE/DX =    0.0                 !
! A94   A(10,47,49)          108.7195         -DE/DX =    0.0                 !
! A95   A(10,47,50)          109.7515         -DE/DX =    0.0                 !
! A96   A(48,47,49)          109.7477         -DE/DX =    0.0                 !
! A97   A(48,47,50)          109.1404         -DE/DX =    0.0                 !
! A98   A(49,47,50)          108.7987         -DE/DX =    0.0                 !
! D1    D(6,1,2,3)            -2.6644         -DE/DX =    0.0                 !
! D2    D(6,1,2,13)          174.7841         -DE/DX =    0.0                 !
! D3    D(8,1,2,3)           176.5777         -DE/DX =    0.0                 !
! D4    D(8,1,2,13)           -5.9738         -DE/DX =    0.0                 !
! D5    D(2,1,6,5)             1.3716         -DE/DX =    0.0                 !
! D6    D(2,1,6,18)         -178.6286         -DE/DX =    0.0                 !
! D7    D(8,1,6,5)          -177.8777         -DE/DX =    0.0                 !
! D8    D(8,1,6,18)            2.1222         -DE/DX =    0.0                 !
! D9    D(2,1,8,10)          -13.2867         -DE/DX =    0.0                 !
! D10   D(2,1,8,17)         -179.3204         -DE/DX =    0.0                 !
! D11   D(6,1,8,10)          165.9705         -DE/DX =    0.0                 !
! D12   D(6,1,8,17)           -0.0632         -DE/DX =    0.0                 !
! D13   D(1,2,3,4)             1.3048         -DE/DX =    0.0                 !
! D14   D(1,2,3,7)          -178.6954         -DE/DX =    0.0                 !
! D15   D(13,2,3,4)         -176.1398         -DE/DX =    0.0                 !
! D16   D(13,2,3,7)            3.8601         -DE/DX =    0.0                 !
! D17   D(1,2,13,15)          -2.185          -DE/DX =    0.0                 !
! D18   D(1,2,13,35)        -115.5061         -DE/DX =    0.0                 !
! D19   D(1,2,13,39)         121.7902         -DE/DX =    0.0                 !
! D20   D(3,2,13,15)         175.1691         -DE/DX =    0.0                 !
! D21   D(3,2,13,35)          61.8481         -DE/DX =    0.0                 !
! D22   D(3,2,13,39)         -60.8557         -DE/DX =    0.0                 !
! D23   D(2,3,4,5)             1.3039         -DE/DX =    0.0                 !
! D24   D(2,3,4,14)         -176.1397         -DE/DX =    0.0                 !
! D25   D(7,3,4,5)          -178.6959         -DE/DX =    0.0                 !
! D26   D(7,3,4,14)            3.8605         -DE/DX =    0.0                 !
! D27   D(3,4,5,6)            -2.6641         -DE/DX =    0.0                 !
! D28   D(3,4,5,9)           176.5793         -DE/DX =    0.0                 !
! D29   D(14,4,5,6)          174.7834         -DE/DX =    0.0                 !
! D30   D(14,4,5,9)           -5.9732         -DE/DX =    0.0                 !
! D31   D(3,4,14,16)         175.1696         -DE/DX =    0.0                 !
! D32   D(3,4,14,27)         -60.853          -DE/DX =    0.0                 !
! D33   D(3,4,14,31)          61.8496         -DE/DX =    0.0                 !
! D34   D(5,4,14,16)          -2.1836         -DE/DX =    0.0                 !
! D35   D(5,4,14,27)         121.7938         -DE/DX =    0.0                 !
! D36   D(5,4,14,31)        -115.5035         -DE/DX =    0.0                 !
! D37   D(4,5,6,1)             1.3719         -DE/DX =    0.0                 !
! D38   D(4,5,6,18)         -178.6279         -DE/DX =    0.0                 !
! D39   D(9,5,6,1)          -177.8786         -DE/DX =    0.0                 !
! D40   D(9,5,6,18)            2.1215         -DE/DX =    0.0                 !
! D41   D(4,5,9,11)          -13.288          -DE/DX =    0.0                 !
! D42   D(4,5,9,12)         -179.3217         -DE/DX =    0.0                 !
! D43   D(6,5,9,11)          165.9705         -DE/DX =    0.0                 !
! D44   D(6,5,9,12)           -0.0633         -DE/DX =    0.0                 !
! D45   D(1,8,10,15)          38.822          -DE/DX =    0.0                 !
! D46   D(1,8,10,43)         -85.74           -DE/DX =    0.0                 !
! D47   D(1,8,10,47)         153.0761         -DE/DX =    0.0                 !
! D48   D(17,8,10,15)       -154.7496         -DE/DX =    0.0                 !
! D49   D(17,8,10,43)         80.6885         -DE/DX =    0.0                 !
! D50   D(17,8,10,47)        -40.4955         -DE/DX =    0.0                 !
! D51   D(5,9,11,16)          38.8215         -DE/DX =    0.0                 !
! D52   D(5,9,11,19)         153.0748         -DE/DX =    0.0                 !
```

```
! D53   D(5,9,11,23)          -85.7425         -DE/DX =    0.0                 !
! D54   D(12,9,11,16)        -154.7499         -DE/DX =    0.0                 !
! D55   D(12,9,11,19)         -40.4967         -DE/DX =    0.0                 !
! D56   D(12,9,11,23)          80.6861         -DE/DX =    0.0                 !
! D57   D(8,10,15,13)         -50.3662         -DE/DX =    0.0                 !
! D58   D(43,10,15,13)         70.4251         -DE/DX =    0.0                 !
! D59   D(47,10,15,13)       -167.0804         -DE/DX =    0.0                 !
! D60   D(8,10,43,44)         176.3371         -DE/DX =    0.0                 !
! D61   D(8,10,43,45)         -64.0234         -DE/DX =    0.0                 !
! D62   D(8,10,43,46)          55.3096         -DE/DX =    0.0                 !
! D63   D(15,10,43,44)         54.8651         -DE/DX =    0.0                 !
! D64   D(15,10,43,45)        174.5046         -DE/DX =    0.0                 !
! D65   D(15,10,43,46)        -66.1624         -DE/DX =    0.0                 !
! D66   D(47,10,43,44)        -64.0787         -DE/DX =    0.0                 !
! D67   D(47,10,43,45)         55.5608         -DE/DX =    0.0                 !
! D68   D(47,10,43,46)        174.8938         -DE/DX =    0.0                 !
! D69   D(8,10,47,48)          59.4631         -DE/DX =    0.0                 !
! D70   D(8,10,47,49)        -179.9395         -DE/DX =    0.0                 !
! D71   D(8,10,47,50)         -61.0459         -DE/DX =    0.0                 !
! D72   D(15,10,47,48)        176.2951         -DE/DX =    0.0                 !
! D73   D(15,10,47,49)        -63.1076         -DE/DX =    0.0                 !
! D74   D(15,10,47,50)         55.7861         -DE/DX =    0.0                 !
! D75   D(43,10,47,48)        -59.4937         -DE/DX =    0.0                 !
! D76   D(43,10,47,49)         61.1037         -DE/DX =    0.0                 !
! D77   D(43,10,47,50)       -180.0027         -DE/DX =    0.0                 !
! D78   D(9,11,16,14)         -50.3637         -DE/DX =    0.0                 !
! D79   D(19,11,16,14)       -167.0772         -DE/DX =    0.0                 !
! D80   D(23,11,16,14)         70.4284         -DE/DX =    0.0                 !
! D81   D(9,11,19,20)          59.4633         -DE/DX =    0.0                 !
! D82   D(9,11,19,21)        -179.9394         -DE/DX =    0.0                 !
! D83   D(9,11,19,22)         -61.0457         -DE/DX =    0.0                 !
! D84   D(16,11,19,20)        176.2949         -DE/DX =    0.0                 !
! D85   D(16,11,19,21)        -63.1078         -DE/DX =    0.0                 !
! D86   D(16,11,19,22)         55.7859         -DE/DX =    0.0                 !
! D87   D(23,11,19,20)        -59.4925         -DE/DX =    0.0                 !
! D88   D(23,11,19,21)         61.1048         -DE/DX =    0.0                 !
! D89   D(23,11,19,22)       -180.0015         -DE/DX =    0.0                 !
! D90   D(9,11,23,24)         176.3343         -DE/DX =    0.0                 !
! D91   D(9,11,23,25)         -64.0263         -DE/DX =    0.0                 !
! D92   D(9,11,23,26)          55.3064         -DE/DX =    0.0                 !
! D93   D(16,11,23,24)         54.8613         -DE/DX =    0.0                 !
! D94   D(16,11,23,25)        174.5007         -DE/DX =    0.0                 !
! D95   D(16,11,23,26)        -66.1666         -DE/DX =    0.0                 !
! D96   D(19,11,23,24)        -64.0825         -DE/DX =    0.0                 !
! D97   D(19,11,23,25)         55.5569         -DE/DX =    0.0                 !
! D98   D(19,11,23,26)        174.8896         -DE/DX =    0.0                 !
! D99   D(2,13,15,10)          32.8129         -DE/DX =    0.0                 !
! D100  D(35,13,15,10)        150.6727         -DE/DX =    0.0                 !
! D101  D(39,13,15,10)        -92.626          -DE/DX =    0.0                 !
! D102  D(2,13,35,36)         -64.2477         -DE/DX =    0.0                 !
! D103  D(2,13,35,37)          56.3958         -DE/DX =    0.0                 !
! D104  D(2,13,35,38)         175.716          -DE/DX =    0.0                 !
! D105  D(15,13,35,36)        177.2478         -DE/DX =    0.0                 !
! D106  D(15,13,35,37)        -62.1087         -DE/DX =    0.0                 !
! D107  D(15,13,35,38)         57.2115         -DE/DX =    0.0                 !
! D108  D(39,13,35,36)         60.2265         -DE/DX =    0.0                 !
! D109  D(39,13,35,37)       -179.13           -DE/DX =    0.0                 !
! D110  D(39,13,35,38)        -59.8098         -DE/DX =    0.0                 !
! D111  D(2,13,39,40)          65.5341         -DE/DX =    0.0                 !
! D112  D(2,13,39,41)        -175.3624         -DE/DX =    0.0                 !
! D113  D(2,13,39,42)         -54.9418         -DE/DX =    0.0                 !
! D114  D(15,13,39,40)       -169.9088         -DE/DX =    0.0                 !
! D115  D(15,13,39,41)        -50.8054         -DE/DX =    0.0                 !
! D116  D(15,13,39,42)         69.6152         -DE/DX =    0.0                 !
! D117  D(35,13,39,40)        -57.4993         -DE/DX =    0.0                 !
! D118  D(35,13,39,41)         61.6041         -DE/DX =    0.0                 !
! D119  D(35,13,39,42)       -177.9752         -DE/DX =    0.0                 !
```

```
 ! D120  D(4,14,16,11)          32.81          -DE/DX =    0.0                 !
 ! D121  D(27,14,16,11)        -92.6305        -DE/DX =    0.0                 !
 ! D122  D(31,14,16,11)        150.6688        -DE/DX =    0.0                 !
 ! D123  D(4,14,27,28)          65.5346        -DE/DX =    0.0                 !
 ! D124  D(4,14,27,29)        -175.3622        -DE/DX =    0.0                 !
 ! D125  D(4,14,27,30)         -54.9413        -DE/DX =    0.0                 !
 ! D126  D(16,14,27,28)       -169.907         -DE/DX =    0.0                 !
 ! D127  D(16,14,27,29)        -50.8038        -DE/DX =    0.0                 !
 ! D128  D(16,14,27,30)         69.617         -DE/DX =    0.0                 !
 ! D129  D(31,14,27,28)        -57.498         -DE/DX =    0.0                 !
 ! D130  D(31,14,27,29)         61.6052        -DE/DX =    0.0                 !
 ! D131  D(31,14,27,30)       -177.9739        -DE/DX =    0.0                 !
 ! D132  D(4,14,31,32)         -64.2477        -DE/DX =    0.0                 !
 ! D133  D(4,14,31,33)          56.3957        -DE/DX =    0.0                 !
 ! D134  D(4,14,31,34)         175.716         -DE/DX =    0.0                 !
 ! D135  D(16,14,31,32)        177.2484        -DE/DX =    0.0                 !
 ! D136  D(16,14,31,33)        -62.1081        -DE/DX =    0.0                 !
 ! D137  D(16,14,31,34)         57.2121        -DE/DX =    0.0                 !
 ! D138  D(27,14,31,32)         60.2262        -DE/DX =    0.0                 !
 ! D139  D(27,14,31,33)       -179.1304        -DE/DX =    0.0                 !
 ! D140  D(27,14,31,34)        -59.8101        -DE/DX =    0.0                 !
```

Repeat geometry optimization for 4a with “tight” convergence constraints

```
******************************************
 Gaussian 03:  IA32W-G03RevC.02 12-Jun-2004
               08-Oct-2007
 ******************************************
 %chk=C:\G03W\Radicals\Oxazene NO\Freq2_Oxaxene_MTDiNO_B3LYP_S1r1.chk
 %mem=8MW
 %nproc=1
 Will use up to    1 processors via shared memory.
 --------------------------------------------------
 # opt=tight freq ub3lyp/6-31g(d) geom=connectivity
 --------------------------------------------------
Step number 136 out of a maximum of 300
SCF Done:  E(UB+HF-LYP) =  -1111.85524353     A.U. after   23 cycles
             Convg  =    0.8097D-08             -V/T =  2.0093
             S**2   =   2.0340
 Annihilation of the first spin contaminant:
 S**2 before annihilation     2.0340,   after     2.0006


Item               Value     Threshold  Converged?
 Maximum Force            0.000001     0.000015     YES
 RMS     Force            0.000000     0.000010     YES
 Maximum Displacement     0.002057     0.000060     NO
 RMS     Displacement     0.000408     0.000040     NO
 Predicted change in Energy=-8.517637D-10
 GradGradGradGradGradGradGradGradGradGradGradGradGradGradGradGradGradGrad

                          Input orientation:
 ---------------------------------------------------------------------
 Center     Atomic     Atomic              Coordinates (Angstroms)
 Number     Number      Type              X           Y           Z
 ---------------------------------------------------------------------
    1          6             0       -0.000059    0.000118   -0.000004
    2          6             0       -0.000055   -0.000040    1.414126
    3          6             0        1.238069   -0.000099    2.060714
    4          6             0        2.456445    0.026621    1.378166
    5          6             0        2.414465    0.083417   -0.034202
    6          6             0        1.196754    0.055937   -0.720186
    7          1             0        1.254203   -0.021954    3.146599
    8          7             0       -1.210488   -0.072256   -0.699288
    9          7             0        3.603619    0.184587   -0.765672
```

```
    10          6           0       -2.456891   -0.447946    0.038743
    11          6           0        4.871757    0.530594   -0.050501
    12          8           0        3.590477    0.250615   -2.042851
    13          6           0       -1.301815    0.057968    2.200652
    14          6           0        3.780954   -0.062081    2.122724
    15          8           0       -2.440103    0.160089    1.315901
    16          8           0        4.892341   -0.128274    1.201130
    17          8           0       -1.235384   -0.086551   -1.977916
    18          1           0        1.180701    0.077700   -1.800478
    19          6           0        6.051857   -0.049864   -0.825331
    20          1           0        6.081998    0.352229   -1.838241
    21          1           0        6.976269    0.204303   -0.299221
    22          1           0        5.962236   -1.138005   -0.874244
    23          6           0        4.958232    2.062630    0.042918
    24          1           0        5.843235    2.349191    0.618881
    25          1           0        5.035055    2.480923   -0.964974
    26          1           0        4.071396    2.490089    0.517863
    27          6           0        3.984129    1.101895    3.112740
    28          1           0        3.247801    1.055849    3.922254
    29          1           0        4.983424    1.029120    3.553984
    30          1           0        3.887425    2.076135    2.628695
    31          6           0        3.879038   -1.402544    2.874614
    32          1           0        3.114522   -1.475515    3.654153
    33          1           0        3.751514   -2.235397    2.177718
    34          1           0        4.865243   -1.487051    3.342620
    35          6           0       -1.376790    1.367306    3.008008
    36          1           0       -0.589414    1.409594    3.766787
    37          1           0       -1.269553    2.227382    2.341419
    38          1           0       -2.348615    1.432452    3.508092
    39          6           0       -1.476100   -1.144716    3.149029
    40          1           0       -0.715927   -1.130638    3.937413
    41          1           0       -2.461741   -1.090166    3.622439
    42          1           0       -1.394519   -2.098795    2.623789
    43          6           0       -2.540884   -1.982578    0.073082
    44          1           0       -3.408659   -2.292903    0.662785
    45          1           0       -2.647337   -2.360163   -0.948103
    46          1           0       -1.640577   -2.427872    0.504277
    47          6           0       -3.659369    0.162023   -0.676730
    48          1           0       -3.720022   -0.199466   -1.703483
    49          1           0       -4.567725   -0.113555   -0.133706
    50          1           0       -3.570758    1.251313   -0.684980
 ---------------------------------------------------------------------
```